Vol. 92 No. 4 pp. 1451–1467 ACTA GEOLOGICA SINICA (English Edition) Aug. 2018

New Insights into the Late Triassic Nadigangri Formation of Northern Qiangtang, Tibet, China: Constraints from U-Pb Ages and Hf Isotopes of Detrital and Magmatic Zircons

LI Xueren[1, 2, 3], WANG Jian[3, 4, *], CHENG Leli[5], FU Xiugen[3, 4] and WANG Yuke[3, 4]

1 *Chinese Academy of Geological Sciences, Beijing 100037, China*
2 *China University of Geosciences (Beijing), Beijing 100083, China*
3 *Key Laboratory for Sedimentary Basin and Oil and Gas Resources, Ministry of Land and Resources, Chengdu, Sichuan 610081, China*
4 *Chengdu Center of Chia Geological Survey, Chengdu, Sichuan 610081, China*
5 *Institute of Mud Logging Technology and Engineering, Yangtze University, Jingzhou, Hubei 434023, China*

Abstract: We report here U-Pb age and *in situ* Hf isotopic results for detrital and magmatic zircons from one conglomerate and four tuffite samples from the Late Triassic Nadigangri Formation across the North Qiangtang depression, Tibet. Coupled with previously published data in the region, this paper proposes new insights into the geochronological framework for the Nadigangri Formation. The deposition ages of tuffite from top to bottom in the Woruo Mountain, Quem Co and Dongqu River, are 203 Ma, 226 Ma, 221.5 Ma and 221.1 Ma, respectively. The detrital zircons yield a younger cluster of ages of 201.5–225 Ma from the conglomerate of the Quem Co Formation. The Late Triassic Nadigangri Formation defines a temporal range approximately between 201 and 225 Ma (Norian-Rhaetian), including three predominant groups of 220–225 Ma , 210–217 Ma and 201–205 Ma, which correspond with the three main rifting episodes of initial rifting, further rifting and final rifting. Positive $\varepsilon_{Hf}(t)$ value and low model ages in younger detrital zircons suggests a juvenile character. However, the Hf isotopes of magmatic zircons display the presence of reworked ancient crust with 1.1–1.8 Ga. These results provide strong constraints not only on the temporal range of the Late Triassic Nadigangri Formation, but also on the onset of the Qiangtang Mesozoic rift basin.

Key words: U-Pb ages, Hf isotope, Nadigangri Formation, Late Triassic, Qiangtang

1 Introduction

The Qiangtang Basin, located in the eastern Tethyan realm, is the biggest petroleum basin in the Qinghai-Tibet Plateau, which is also recognised as the best-developed region of Mesozoic marine sediments in China (Zhao and Li, 2000; Wang et al., 2004). Generally, basin evolution plays a critical role in petroleum exploration and development. It is considered that the Mesozoic Qiangtang Basin is a large-scale composite basin, superimposed by foreland and rift basins in the Triassic and Jurassic, respectively (Wang Jian et al., 2009; Fu et al., 2016a). The foreland basin of the Northern Qiangtang experienced shrinkiage and disappeared due to tectonic uplift and regional regression in the early Late Triassic. Due to the opening of the Bangong–Nujiang Tethyan Ocean during the Late Triassic, a series of rifts occurred with massive volcanic eruptions, forming three main rift troughs (1.Wanwanliang–Quem Co; 2.Xiaochaka–Biluo Co; 3.Tu Co) in the North Qiangtang depression (Fig. 1b, Tan Fuwen et al., 2016). The Jurassic rift basin was therefore developed on the base of the rifting basement at the top of the Upper Triassic strata.

The Nadigangri Formation, mainly composed of basalt, rhyolite and felsic tuffite, is distributed with an approximately NW-SE trend along three main depressions in the Qiangtang Basin (Fig. 1b). Furthermore, the exposure of the Nadigangri Formation matches well with the rifting basement of the Upper Triassic strata, which indicates that it was a large-scale volcanic-sedimentary event related to rifting in the region. These volcanic rocks

* Corresponding author. E-mail: w1962jian@163.com

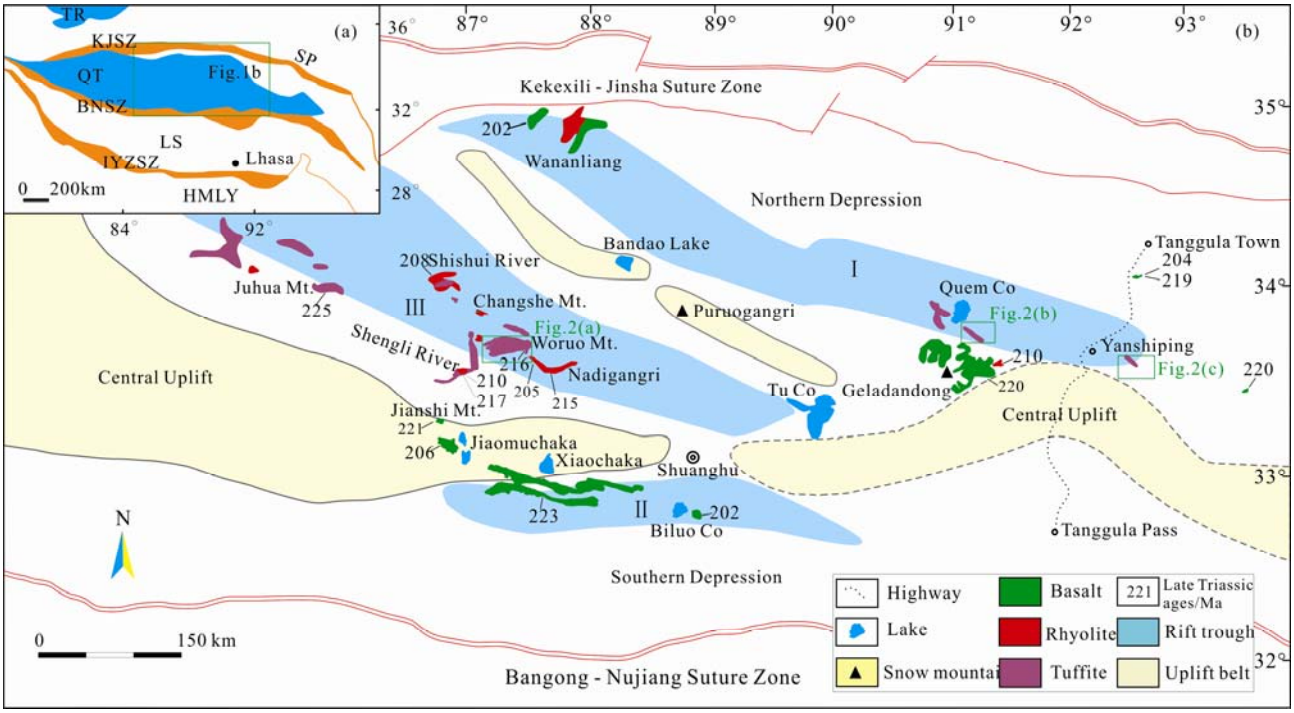

Fig. 1. Schematic maps showing (a) Map of the Tibetan plateau showing major Terranes (modified from Fu et al. (2016a)) (b) Tectonic outline of the Qiangtang Basin and distribution of the rocks of the Nadigangri Formation (modified from Tan et al. (2016)).
TR, Tarim Basin; KJSZ, Kekexili–Jinsha Suture Zone; SP, Songpan–Ganzi; QT, Qiangtang; BNSZ, Bangong–Nujiang Suture Zone; LS, Lhasa; IYZSZ, Indus–Yarlung Zangbo Suture Zone; HMLY, Himalayas.

have a bimodal affinity that is typical of an extensional setting, and the basalts are geochemically consistent with within-plate continental basalt formed in an extensional setting. With respect to the Late Triassic sedimentation, the Nadigangri Formation consists of alluvial and fluvial volcaniclastic deposits associated with continental explosive volcanic facies, which are overlain by littoral to shallow-marine facies of the Early Jurassic sedimentary successions (Wang Jian et al., 2004; Fu et al., 2010a). Furthermore, the pre-Nadigangri paleo-weathered crust is overlain unconformably by the Nadigangri Formation (Zhu Tongxing et al., 2002; Wang Jian et al., 2007a; Chen Wenxi et al., 2007; Fu Xiugen et al., 2009). Therefore, the Nadigangri volcanic-sedimentary rocks represent the beginning of the filling in of the rift basin and the period represented by Nadigangri can be regarded as an independent phase of the rifting. A great deal of research, including opening timing, tectonic setting and basin nature, has been done on the onset of the rift basin over the last decade (Wang Jian et al., 2004, 2007b, 2008, 2009, 2018; Fu et al., 2010a, 2016a; Tan Fuwen et al., 2016). The available data shows that the eruptive and depositional ages of volcanic-sedimentary rocks of the Nadigangri Formation range from ca. 220 to 205 Ma (Fu Xiugen et al., 2010b; Wu et al., 2015). However, previous studies focused mainly on the scattered lavas, little being known about the pyroclastic-sedimentary rocks, especially the tuffite. The tuffite is not only a pyroclastic rock but also a sedimentary rock with horizontal bedding, according to petrological classification. The volcanic rocks are often poorly-preserved in the basin due to rifting, tectonic uplift, late burial and erosion. In contrast, the tuffite preserved in sedimentary successions has been shown to contain a more complete time record of volcanism and the stratigraphic sequence (Perkins and Nash, 2002). The volcanic-sedimentary successions remaining in the depressions of the basin may record the processes of the beginning, the peak and the end of the Nadigangri phase. It is possible to accurately determine how long the deposition has lasted through ages of both the top and the bottom of the tuffite.

In this paper, we present U-Pb geochronological and Hf isotopic data from detrital and magmatic zircons from the tuffite and quartz conglomerate in the North Qiangtang depression. These data, in combination with previous results, are used to develop a detailed temporal framework for the Nadigangri phase, and to provide new constraints on the crustal evolution of the Qiangtang Basin.

2 Geological Settings and Sampling

The Tibetan Plateau consists of four main terranes: the Songpan–Ganzi, the Qiangtang, the Lhasa, and the Himalaya, which are separated by the Kekexili–Jinsha

Suture Zone (KJSZ), the Bangong Lake–Nujiang Suture Zone (BNSZ), and the Indus-Yarlung Zangbo Suture Zone (IYZSZ), respectively (Fig. 1a; Pearce and Mei, 1988; Yin and Harrison, 2000; Kapp et al., 2003). The Qiangtang Basin, bounded by the KJSZ to the north and the BNSZ to the south, can be subdivided into the North Qiangtang depression and the South Qiangtang depression by an uplift (the west is a physical uplift, while the east is a hidden one) in the central Qiangtang Basin (Fig. 1b; Wang Jian et al., 2004).

Based on lithofacies analysis and paleogeographic maps, the North Qiangtang depression experienced a foreland basin evolution during the Early-Late Triassic and a rift basin evolution during the Late Triassic-Early Cretaceous (Wang Jian et al., 2010; Fu et al., 2016a). In the foreland stage, the Late Triassic Xiaochaka Formation was deposited in the basin, and it is subdivided into three members in an ascending order: clastics, carbonates, and coal-bearing clastics. Subsequently, a relatively short depositional hiatus has been recorded prior to the onset of the Nadigangri phase, when paleo-weathered crusts occur widely throughout the Juhua Mountain, Xiaochaka, Shengli River and Zangxia River regions in the Qiangtang Basin (Chen et al., 2007; Wang et al., 2007a; Fu et al., 2009). The stratum of the rift basin in the North Qiangtang depression is primarily made up of Late Triassic volcanic-sedimentary rocks of the Nadigangri Formation and Jurassic–Cretaceous clastics and carbonates including the Quem Co Formation, Buqu Formation, Xiali Formation, Suowa Formation and the Xueshan Formation (Fig. 2; Fu

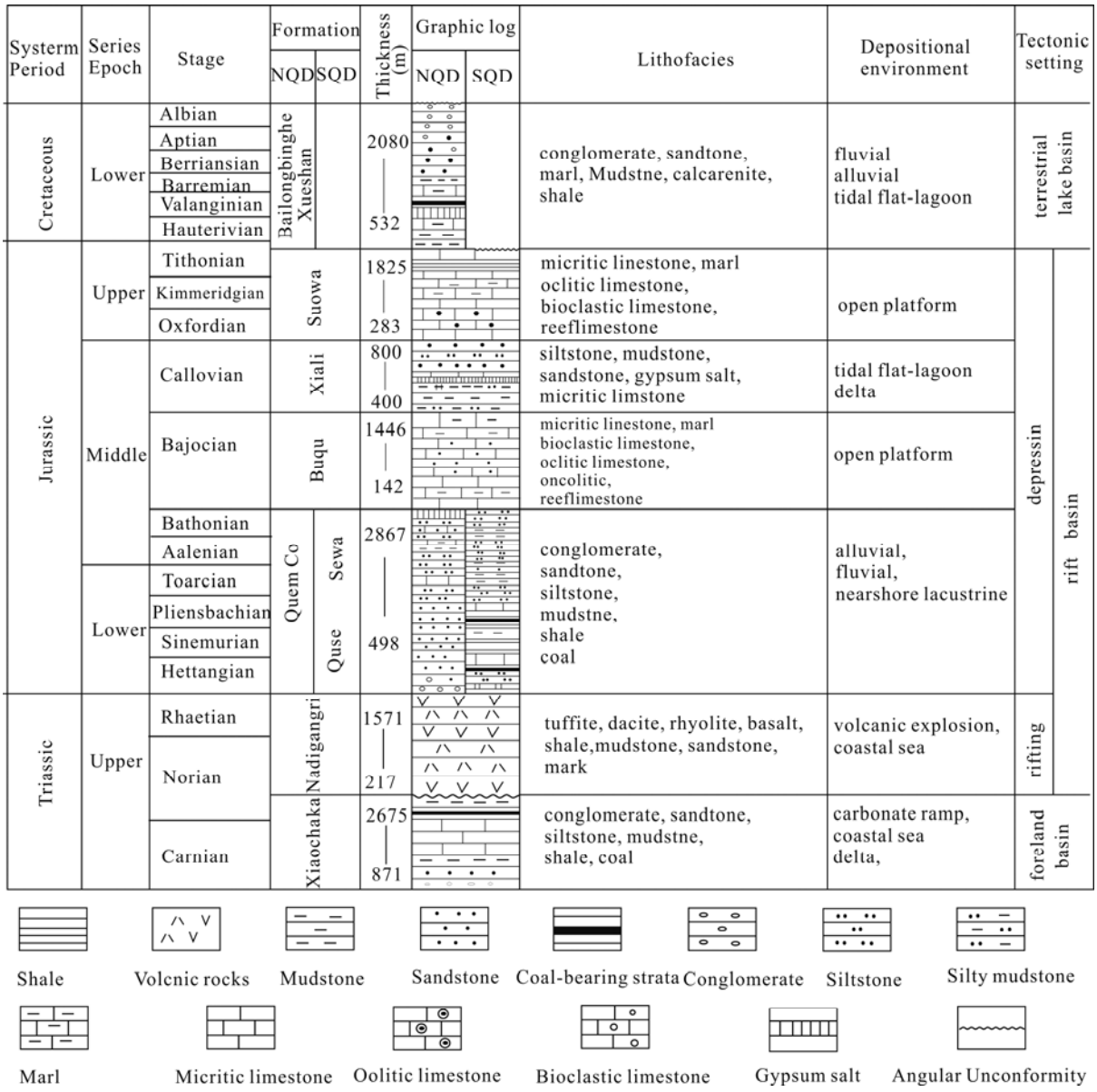

Fig. 2. A schematic diagram showing the major stratigraphic units of the Qiangtang Basin (modified from Fu et al. (2016a)). NQD─North Qiangtang depression; SQD─South Qiangtang depression.

et al., 2016a; Song et al., 2017). The Nadigangri Formation, primarily consisting of basic and felsic lavas, volcanic breccia, terrigenous clastics with tuffite interlayers, is underlain by the Xiaochaka Formation and coeval strata.

In the present study, we focus mainly on the tuffite interlayers of the volcanic-sedimentary successions, most of which crop out in the Shishui River, Woruo Mountain, Fang Lake and the Nadigangri regions in the west and Quem Co, Tuotuo River, Moyun Country and the Yanshiping areas in the east of the North Qiangtang depression, respectively. Three representative sections were selected to provide available constraints on the temporal range of the Nadigangri stage from three rift troughs of the North Qiangtang depression (Fig. 3). The tuffite interlayers are generally several centimeters to tens of meters in thickness with horizontal bedding. Samples 16R1-1 and 16R1-2 were collected from the bottom and the top of the Woruo Mountain section, respectively. Sample 16R1-1 is tuffaceous siltstone intercalated with limestone breccia (Fig. 4a) and Sample 16R1-2 is a light green dacitic tuffite which is dominated by volcanic ash (Fig. 4b–c). Samples 15R1 and 15K1 were collected from the bottom and the top of the Quem Co section, respectively. The bottom, underlain conformably by the Xiaochaka Formation, is a green rhyolitic crystal lithic tuffite, with a typical ash texture with minor terrigenous clasts (<10%) and the top of the Quem Co Formation is underlain unconformably by the Nadigangri Formation, consists of a red polymictic conglomerate, which is mainly composed of quartz gravels (Fig. 4d–e). Only sample 15R2 was collected from the bottom of the Dongqu River section, due to the absence of the top, but the sample is an extremely pure rhyolitic crystal tuffite (Fig. 4f).

3 Analytical Methods

3.1 Zircon U–Pb dating by LA-ICP-MS

Zircons for LA-MC-ICP-MS U-Pb dating were separated from crushed rock by using conventional heavy liquid and magnetic techniques, and purified by handpicking under a binocular microscope. They were

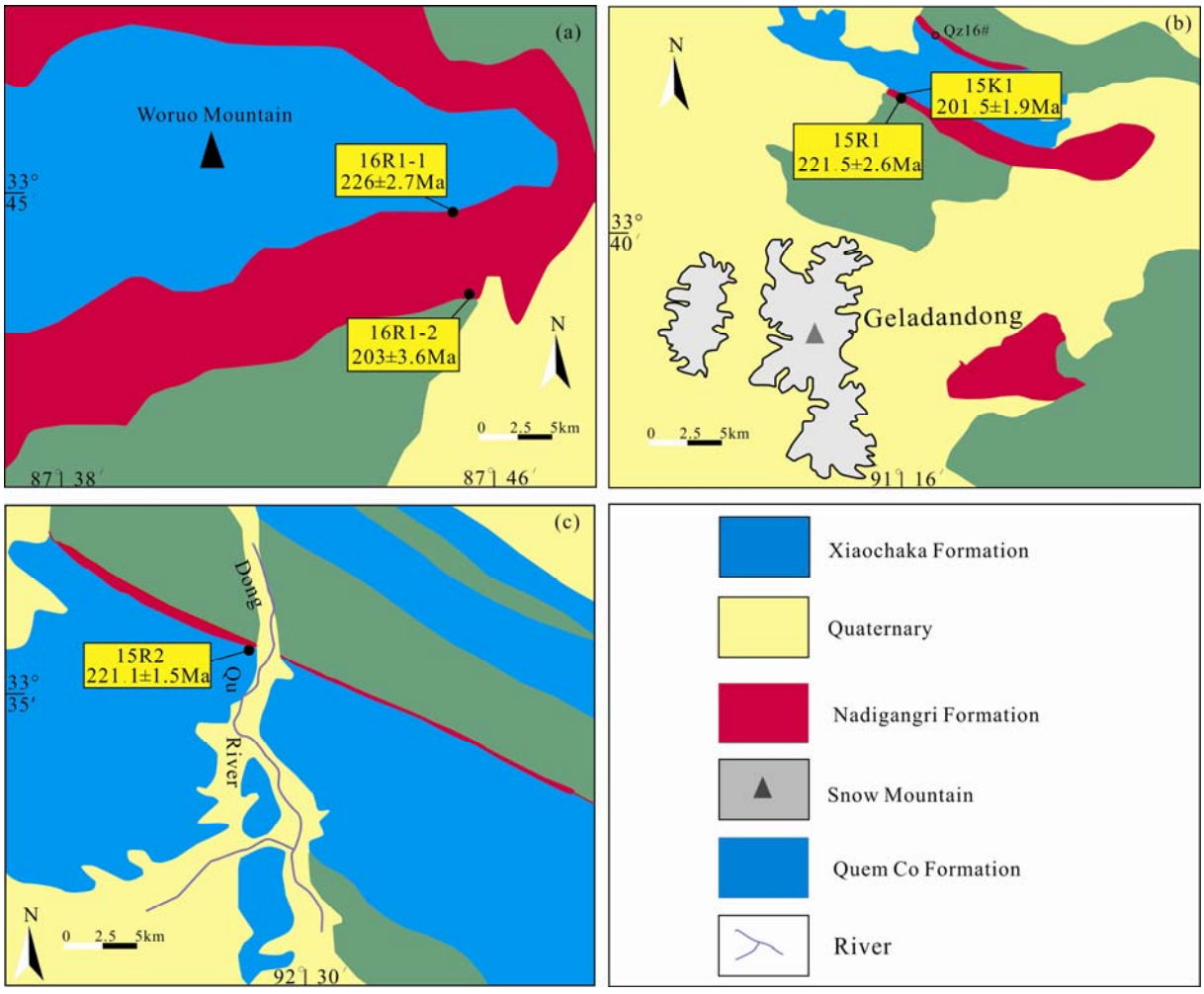

Fig. 3. Simplified geological map of the Woruo Mountain, Quem Co and Dongqu River areas, and the sampling locations in those areas.

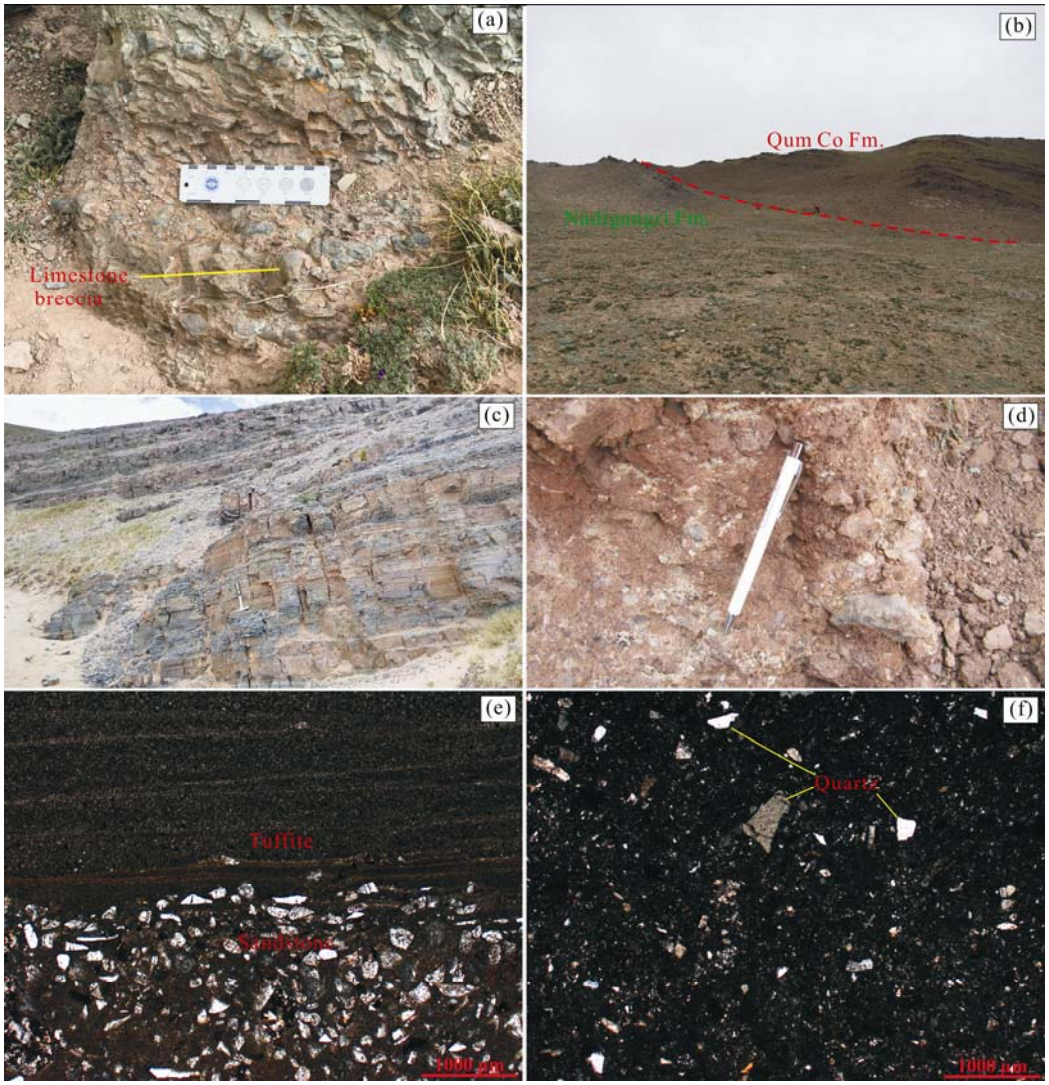

Fig. 4. Field photographs (a–d) and photomicrographs (e–f) of the tuffite and Jurassic conglomerate in the Woruo Mountain, Quem Co and Dongqu River areas.
(a), Tuffaceous siltstone intercalated with limestone breccia; (b), contact boundary of the Nadigangri Formation and Quem Co Formations in the Woruo Mountain section; (c), green tuffite with parallel bedding in the Quem Co section; (d), red conglomerate of Quem Co; (e), photomicrographs of sample 15R1 in the lowermost part of the sequence, showing contact boundary between the Nadigangri and the Xiaochaka Formations; (f), photomicrographs of sample 15R2 in the lowermost part of the sequence.

mounted in epoxy resin and polished to half their thickness to expose the core of the grains. To analyze the internal structures of the zircons accurately, and determine domains for dating, cathodoluminescence (CL) images were obtained using an GEOL 7100-Gatan scanning electron microscope at the Beijng Geoanalysis Co., Ltd. CL images of the analyzed zircon grains are illustrated in Fig. 5. U-Pb dating by LA-ICP-MS was performed at the State Key Laboratory of Geological Processes and Mineral Resources, the Chinese University of Geosciences, Wuhan. Laser sampling was performed using a GeoLas 2005 System. Helium was used as a carrier gas. An Agilent 7500a ICP-MS instrument was used to acquire ion -signal intensities. Detailed operating conditions for the laser and the ICP-MS instrument can be found in Liu et al. (2008). Zircon 91500 was used as an external standard for the matrix-matched calibration of U-Pb dating, and was analysed twice every five–eight analyses. NISTSRM 612 reference glasses were analyzed as an external standard to calibrate trace element contents. Off-line isotope ratios were calculated by ICPMSDataCal10.2 (Liu et al., 2010). The weighted mean age calculations, concordia diagrams and probability density plots were generated using ISOPLOT 3.7 (Ludwig, 2012). Results are presented in Table 1.

3.2 Zircon Hf isotopic analysis by LA-MC-ICP-MS

In situ zircon Hf isotopic analyses were conducted at the State Key Laboratory of Geological Processes and Mineral Resources, the Chinese University of Geosciences

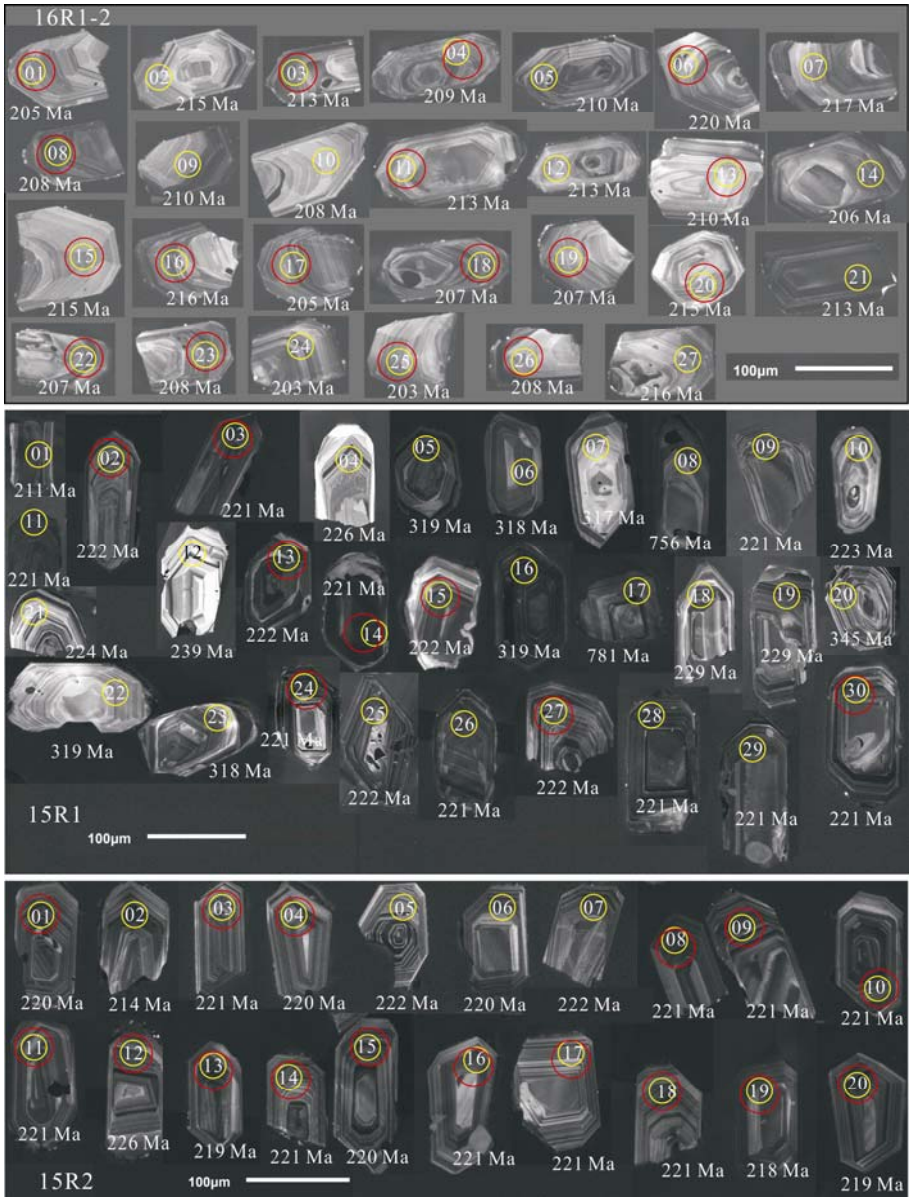

Fig. 5. Representative cathodoluminescence (CL) images of zircons of the tuffite from the Woruo Mountain, Quem Co and Dongqu River areas, with analytical numbers, U-Pb ages, and $\varepsilon_{Hf}(t)$ values.
The location of U-Pb analyses are shown by yellow circles, and *in situ* Hf isotope spots are shown by red circles.

(Wuhan), using a Neptune Plus MC-ICP-MS equipped with a GeoLas 2005 laser-ablation system. Zircon 91500 and GJ-1were used as reference standards, with a recommended $^{176}Hf/^{177}Hf$ ratio of 0.282307±0.000031 (2σ) (Wu Fuyuan et al., 2006) and 0.282000±0.000005 (2σ) (Morel et al., 2008), respectively. Hf isotopic analyses were located on the same (or as close as possible to) spots used for U-Pb dating, with spot sizes of 60 μm in diameter. More details on operating and calibration procedures can be found in Hu et al. (2012). The initial $^{176}Hf/^{177}Hf$ ratio was calculated according to the weighted mean age, and the$\varepsilon_{Hf}(t)$ value was calculated with reference to the chondritic reservoir (CHUR) at the time of the zircon growth from the magmas (ratios of $^{176}Hf/^{177}Hf$=0.282772 and $^{176}Lu/^{177}Hf$=0.0332; Blichert-Toft and Albarède, 1997). One-stage model ages (TDM) were calculated relative to depleted mantle with a present-day ($^{176}Hf/^{177}Hf)_{DM}$=0.28325 and ($^{176}Lu/^{177}Hf)_{DM}$=0.0384 (Griffin et al., 2000). Two-stage model ages (TDM2) were calculated assuming $^{176}Lu/^{177}Hf$ = 0.015 for the average continental crust (Griffin et al., 2002). Off-line selection and integration of analytical signals were also performed using ICPMSDataCal10.2 (Liu et al., 2010). The Hf isotopic data are listed in Table 2).

Table 1 Zircon LA-ICP-MS U-Pb data of tuffie and conglomerate samples from the North Qiangtang depression, Tibet

Spot	w_B (10^{-6})		Th/U	Corrected isotope ratios						Isotope ages (Ma)					
	Th	U		$^{207}Pb/^{206}U$	1σ	$^{207}Pb/^{235}U$	1σ	$^{206}Pb/^{238}U$	1σ	$^{207}Pb/^{206}Pb$	1σ	$^{207}Pb/^{235}U$	1σ	$^{206}Pb/^{238}U$	1σ
16R1-1-1	334	394	0.85	0.0716	0.0022	0.7007	0.0210	0.0709	0.0006	974	63.0	539	12.5	442	3.6
16R1-1-2	629	726	0.87	0.1843	0.0079	1.2461	0.0712	0.0464	0.0009	2692	70.4	822	32.2	293	5.3
16R1-1-3	326	535	0.61	0.0540	0.0015	0.5277	0.0140	0.0704	0.0006	372	61.1	430	9.3	438	3.7
16R1-1-4	114	275	0.41	0.0578	0.0025	0.2840	0.0122	0.0356	0.0004	520	89.8	254	9.6	226	2.7
16R1-1-5	251	397	0.63	0.0514	0.0019	0.2826	0.0101	0.0396	0.0004	261	83.3	253	8.0	250	2.5
16R1-1-6	59.4	161	0.37	0.0501	0.0020	0.5000	0.0209	0.0714	0.0008	198	99.1	412	14.2	445	5.0
16R1-1-7	133	253	0.52	0.0627	0.0022	0.6296	0.0226	0.0721	0.0008	698	75.9	496	14.1	449	4.6
16R1-1-8	255	1083	0.23	0.0778	0.0019	0.9456	0.0217	0.0876	0.0008	1143	49.2	676	11.4	541	4.6
16R1-1-9	238	415	0.57	0.0554	0.0016	0.5535	0.0160	0.0719	0.0007	428	69.4	447	10.5	447	4.3
16R1-1-10	104	222	0.47	0.0701	0.0032	0.3519	0.0152	0.0365	0.0005	931	93.4	306	11.4	231	3.1
16R1-1-11	75.3	241	0.31	0.1179	0.0038	2.6539	0.0975	0.1597	0.0021	1924	58.3	1316	27.1	955	11.8
16R1-1-12	162	363	0.45	0.0473	0.0026	0.1189	0.0066	0.0180	0.0002	64.9	126	114	5.9	115	1.6
16R1-1-13	218	614	0.36	0.1507	0.0104	1.9840	0.1773	0.0821	0.0017	2354	118	1110	60.4	509	10.4
16R1-1-14	255	478	0.53	0.0559	0.0019	0.2972	0.0117	0.0381	0.0006	456	77.8	264	9.2	241	3.6
16R1-1-15	192	314	0.61	0.0636	0.0015	1.0426	0.0254	0.1185	0.0012	731	56.5	725	12.6	722	6.9
16R1-1-16	168	311	0.54	0.0715	0.0016	1.6092	0.0355	0.1625	0.0014	972	44.4	974	13.8	971	8.0
16R1-1-17	120	105	1.14	0.0513	0.0032	0.3038	0.0182	0.0433	0.0006	257	141	269	14.2	273	3.8
16R1-2-1	539	776	0.70	0.0512	0.0027	0.2279	0.0115	0.0324	0.0004	250	120.4	208	9.5	205	2.6
16R1-2-2	683	1445	0.47	0.0535	0.0021	0.2433	0.0095	0.0328	0.0003	350	88.9	221	7.7	208	2.2
16R1-2-3	401	600	0.67	0.0511	0.0030	0.2376	0.0133	0.0339	0.0005	243	135.2	216	10.9	215	2.8
16R1-2-4	345	552	0.63	0.0551	0.0034	0.2559	0.0155	0.0340	0.0005	417	137.0	231	12.5	215	2.9
16R1-2-5	936	1846	0.51	0.0496	0.0018	0.2282	0.0083	0.0332	0.0003	189	80.5	209	6.9	210	2.0
16R1-2-6	421	813	0.52	0.0471	0.0025	0.2210	0.0118	0.0340	0.0004	53.8	122.2	203	9.8	216	2.6
16R1-2-7	882	971	0.91	0.0517	0.0023	0.2385	0.0103	0.0336	0.0004	333	103.7	217	8.4	213	2.6
16R1-2-8	240	378	0.64	0.0515	0.0051	0.2348	0.0256	0.0328	0.0006	261	229.6	214	21.0	208	3.9
16R1-2-9	901	1315	0.69	0.0504	0.0024	0.2243	0.0104	0.0323	0.0004	213	109.2	206	8.6	205	2.4
16R1-2-10	565	1042	0.54	0.0504	0.0027	0.2283	0.0118	0.0330	0.0004	213	124.1	209	9.8	209	2.6
16R1-2-11	437	762	0.57	0.0508	0.0035	0.2323	0.0148	0.0335	0.0005	235	161.1	212	12.2	213	3.1
16R1-2-12	954	2900	0.33	0.0477	0.0017	0.2152	0.0073	0.0327	0.0003	87.1	81.5	198	6.1	207	1.9
16R1-2-13	1943	2930	0.66	0.0521	0.0017	0.2384	0.0073	0.0332	0.0003	287	74.1	217	6.0	210	2.0
16R1-2-14	366	559	0.66	0.0555	0.0041	0.2465	0.0156	0.0337	0.0006	435	166.7	224	12.7	213	3.6
16R1-2-15	473	725	0.65	0.0501	0.0032	0.2218	0.0135	0.0326	0.0004	198	148.1	203	11.2	207	2.8
16R1-2-16	697	1108	0.63	0.0502	0.0029	0.2403	0.0129	0.0347	0.0005	211	133.3	219	10.6	220	2.8
16R1-2-17	361	402	0.90	0.0530	0.0040	0.2456	0.0189	0.0331	0.0006	328	174.1	223	15.4	210	4.0
16R1-2-18	702	1280	0.55	0.0470	0.0021	0.2201	0.0092	0.0338	0.0004	55.7	98.1	202	7.7	215	2.6
16R1-2-19	542	1249	0.43	0.0538	0.0026	0.2520	0.0120	0.0342	0.0004	361	111.1	228	9.8	217	2.6
16R1-2-20	952	1931	0.49	0.0496	0.0020	0.2221	0.0086	0.0324	0.0003	176	125.0	204	7.1	206	2.0
16R1-2-21	1500	3648	0.41	0.0586	0.0019	0.2746	0.0097	0.0335	0.0003	554	76.8	246	7.8	213	2.1
16R1-2-22	867	1921	0.45	0.0525	0.0019	0.2359	0.0084	0.0326	0.0003	306	76.8	215	6.9	207	2.0
16R1-2-23	771	1472	0.52	0.0535	0.0023	0.2423	0.0103	0.0328	0.0004	350	100.9	220	8.4	208	2.2
16R1-2-24	699	1100	0.64	0.0519	0.0026	0.2287	0.0114	0.0320	0.0004	280	116.7	209	9.4	203	2.5
16R1-2-25	545	800	0.68	0.0545	0.0031	0.2387	0.0133	0.0320	0.0004	391	132.4	217	10.9	203	2.7
16R1-2-26	204	393	0.52	0.0486	0.0044	0.2108	0.0182	0.0328	0.0006	128	200.0	194	15.3	208	3.9
16R1-2-27	335	535	0.63	0.0466	0.0038	0.2148	0.0164	0.0340	0.0005	33.4	179.6	198	13.7	216	3.3
15R1-1	230	251	0.80	0.0539	0.0034	0.2553	0.0195	0.0333	0.0010	365	144.4	231	15.8	211	6.4
15R1-2	385	483	0.57	0.0464	0.0026	0.2326	0.0115	0.0350	0.0014	17	129.6	212	9.5	222	8.4
15R1-3	358	625	0.96	0.0437	0.0023	0.2184	0.0111	0.0349	0.0012	error	error	201	9.2	221	7.5
15R1-4	221	231	0.71	0.0561	0.0047	0.2788	0.0228	0.0357	0.0010	457	188.9	250	18.1	226	6.3
15R1-5	793	1110	0.70	0.0525	0.0021	0.3783	0.0143	0.0507	0.0009	306	90.7	326	10.5	319	5.6
15R1-6	236	336	0.90	0.0489	0.0027	0.3449	0.0181	0.0506	0.0010	142.7	163.9	301	13.7	318	6.2
15R1-7	210	234	0.48	0.0505	0.0033	0.3473	0.0223	0.0505	0.0015	220	150.0	303	16.8	317	9.2
15R1-8	106	221	1.04	0.0616	0.0025	1.0772	0.0404	0.1245	0.0021	657	87.0	742	19.8	756	12.0
15R1-9	239	230	1.14	0.0528	0.0025	0.2522	0.0121	0.0348	0.0007	320	112.0	228	9.8	221	4.2
15R1-10	314	275	0.70	0.0784	0.0100	0.3625	0.0356	0.0351	0.0012	1158	254.2	314	26.6	223	7.4
15R1-11	191	272	1.62	0.0544	0.0022	0.2709	0.0106	0.0349	0.0007	391	92.6	243	8.5	221	4.6
15R1-12	313	193	0.63	0.0450	0.0058	0.2416	0.0304	0.0378	0.0012	error	error	220	24.8	239	7.7
15R1-13	545	868	0.48	0.0513	0.0023	0.2559	0.0135	0.0350	0.0015	254	103.7	231	10.9	222	9.1
15R1-14	360	746	0.92	0.0493	0.0022	0.2428	0.0114	0.0349	0.0010	161	105.5	221	9.3	221	6.3
15R1-15	184	201	0.42	0.0532	0.0030	0.3786	0.0232	0.0507	0.0014	345	123.1	326	17.1	319	8.5
15R1-16	407	971	0.84	0.0490	0.0027	0.2408	0.0155	0.0350	0.0011	150	129.6	219	12.7	222	7.0
15R1-17	235	280	1.36	0.0630	0.0033	1.1265	0.0630	0.1288	0.0019	707	109.2	766	30.1	781	10.9
15R1-18	280	206	0.83	0.0542	0.0036	0.2874	0.0173	0.0361	0.0008	388.9	143.5	257	13.6	229	4.8
15R1-19	209	253	1.56	0.0506	0.0024	0.2448	0.0125	0.0347	0.0006	233	111.1	222	10.2	220	3.6
15R1-20	281	180	1.73	0.0521	0.0023	0.3925	0.0169	0.0550	0.0010	300	100.0	336	12.4	345	5.9
15R1-21	320	185	0.55	0.0439	0.0039	0.2351	0.0181	0.0353	0.0013	error	error	214	14.8	224	8.3
15R1-22	104	191	0.77	0.1080	0.0169	0.5789	0.0657	0.0507	0.0042	1766	289.0	464	42.2	319	25.6
15R1-23	307	398	1.24	0.0506	0.0019	0.3558	0.0150	0.0506	0.0007	233	88.9	309	11.2	318	4.4
15R1-24	271	218	0.61	0.0559	0.0043	0.2604	0.0181	0.0348	0.0009	455.6	174.1	235	14.6	221	5.7
15R1-25	171	280	0.51	0.0495	0.0030	0.2362	0.0142	0.0350	0.0007	172	137.9	215	11.7	222	4.4
15R1-26	361	701	0.41	0.0530	0.0019	0.2571	0.0117	0.0349	0.0008	332	78.7	232	9.4	221	5.2

Table 1 Continued 1

Spot	w_B (10^{-6})		Th/U	Corrected isotope ratios						Isotope ages (Ma)					
	Th	U		$^{207}Pb/^{206}U$	1σ	$^{207}Pb/^{235}U$	1σ	$^{206}Pb/^{238}U$	1σ	$^{207}Pb/^{206}Pb$	1σ	$^{207}Pb/^{235}U$	1σ	$^{206}Pb/^{238}U$	1σ
15R1-27	281	681	0.46	0.0821	0.0028	0.3966	0.0140	0.0350	0.0005	1250	62.8	339	10.2	222	3.2
15R1-28	518	1125	0.51	0.1822	0.0099	0.9693	0.0627	0.0350	0.0009	2673	90.6	688	32.3	221	5.8
15R1-29	387	759	0.63	0.0470	0.0030	0.2230	0.0149	0.0349	0.0007	56	138.9	204	12.4	221	4.2
15R1-30	645	1029	0.63	0.0502	0.0055	0.2273	0.0233	0.0349	0.0009	211.2	227.8	208	19.3	221	5.8
15K1-1	153	111	1.38	0.1606	0.0041	10.4256	0.2724	0.4632	0.0057	2462	44.0	2473	24.3	2454	25.0
15K1-2	32	60	0.54	0.1642	0.0038	11.4728	0.2632	0.4996	0.0052	2499	38.4	2562	21.5	2612	22.3
15K1-3	137	571	0.24	0.1119	0.0021	4.6798	0.0891	0.2984	0.0027	1831	34.4	1764	16.0	1684	13.4
15K1-4	26	676	0.04	0.1460	0.0034	6.9765	0.3040	0.3291	0.0087	2300	39.0	2108	38.7	1834	42.3
15K1-5	69	111	0.62	0.1031	0.0042	1.3721	0.0522	0.0989	0.0025	1680.6	74.1	877	22.4	608	14.4
15K1-6	108	216	0.50	0.0581	0.0018	0.5520	0.0160	0.0685	0.0009	600	73.1	446	10.5	427	5.2
15K1-7	67	136	0.49	0.0714	0.0043	0.3305	0.0181	0.0347	0.0008	969	124.5	290	13.8	220	4.7
15K1-8	109	289	0.38	0.1564	0.0035	8.2936	0.1914	0.3786	0.0048	2418	38.0	2264	21.0	2070	22.4
15K1-9	216	561	0.38	0.0565	0.0020	0.3033	0.0101	0.0385	0.0005	472	77.8	269	7.9	244	3.2
15K1-10	370	936	0.40	0.0537	0.0019	0.2425	0.0079	0.0324	0.0003	361.2	81.5	221	6.5	205	2.0
15K1-11	664	868	0.77	0.0502	0.0021	0.2438	0.0093	0.0349	0.0004	211	98.1	221	7.6	221	2.5
15K1-12	198	482	0.41	0.0633	0.0030	0.5321	0.0243	0.0598	0.0010	720	101.8	433	16.1	374	6.1
15K1-13	225	735	0.31	0.0513	0.0021	0.2402	0.0091	0.0334	0.0003	254	96.3	219	7.4	212	2.1
15K1-14	239	835	0.29	0.0499	0.0019	0.2356	0.0079	0.0338	0.0003	191	87.0	215	6.5	214	1.9
15K1-15	85	237	0.36	0.1154	0.0031	4.8828	0.1294	0.3027	0.0040	1887.0	54.5	1799	22.4	1705	19.6
15K1-16	100	295	0.34	0.1104	0.0025	5.0052	0.1061	0.3245	0.0035	1807	40.4	1820	18.0	1811	17.2
15K1-17	133	402	0.33	0.0562	0.0019	0.3465	0.0106	0.0448	0.0007	457	74.1	302	8.0	283	4.1
15K1-18	119	283	0.42	0.1605	0.0026	10.3054	0.1930	0.4599	0.0067	2461	26.4	2463	17.4	2439	29.5
15K1-19	347	972	0.36	0.0629	0.0013	0.2826	0.0057	0.0324	0.0004	706	46.3	253	4.5	205	2.4
15K1-20	412	287	1.44	0.0797	0.0016	1.5643	0.0503	0.1414	0.0040	1190.7	38.6	956	19.9	853	22.3
15K1-21	157	368	0.43	0.1229	0.0018	4.8158	0.0896	0.2791	0.0031	1999	25.9	1788	15.7	1587	15.8
15K1-22	60	114	0.53	0.0779	0.0038	0.6093	0.0291	0.0593	0.0029	1144	96.3	483	18.4	371	17.4
15K1-23	482	906	0.53	0.0526	0.0011	0.2484	0.0052	0.0339	0.0004	322	52.8	225	4.3	215	2.2
15K1-24	123	222	0.56	0.0703	0.0024	0.3884	0.0141	0.0395	0.0006	939	69.6	333	10.3	250	4.0
15K1-25	112	398	0.28	0.1124	0.0016	4.2212	0.0774	0.2694	0.0040	1838.9	25.9	1678	15.1	1538	20.2
15K1-26	176	244	0.72	0.1553	0.0091	1.5398	0.1349	0.0748	0.0046	2405	99.8	946	53.9	465	27.7
15K1-27	494	899	0.55	0.0584	0.0012	0.2762	0.0052	0.0341	0.0003	543	44.4	248	4.1	216	2.1
15K1-28	354	905	0.39	0.0525	0.0011	0.2359	0.0046	0.0324	0.0003	306	48.1	215	3.8	206	1.8
15K1-29	83	159	0.52	0.0535	0.0027	0.2390	0.0124	0.0326	0.0005	350	114.8	218	10.1	207	3.4
15K1-30	235	255	0.92	0.0516	0.0015	0.3560	0.0104	0.0501	0.0007	264.9	66.7	309	7.8	315	4.2
15K1-31	208	295	0.71	0.1027	0.0016	4.1132	0.0758	0.2883	0.0039	1674	23.3	1657	15.1	1633	19.4
15K1-32	209	96	2.19	0.0751	0.0021	1.4958	0.0412	0.1450	0.0024	1072	54.2	929	16.8	873	13.6
15K1-33	305	694	0.44	0.0814	0.0028	0.4052	0.0161	0.0352	0.0004	1231	68.1	345	11.6	223	2.5
15K1-34	158	328	0.48	0.1148	0.0016	5.0209	0.0852	0.3143	0.0036	1877	24.2	1823	14.4	1762	17.9
15K1-35	415	884	0.47	0.0555	0.0012	0.2609	0.0056	0.0340	0.0004	431.5	48.1	235	4.5	215	2.2
15K1-36	184	515	0.36	0.0555	0.0018	0.2662	0.0084	0.0349	0.0006	432	69.4	240	6.7	221	3.8
15K1-37	34	75	0.45	0.0613	0.0030	0.4720	0.0222	0.0572	0.0013	650	105.5	393	15.3	358	7.9
15K1-38	158	93	1.70	0.0661	0.0019	0.9911	0.0306	0.1092	0.0023	809	63.9	699	15.6	668	13.3
15K1-39	210	663	0.32	0.0536	0.0012	0.2446	0.0054	0.0329	0.0003	354	84.3	222	4.4	209	2.1
15K1-40	120	235	0.51	0.0572	0.0018	0.3122	0.0100	0.0395	0.0006	501.9	70.4	276	7.7	250	3.5
15K1-41	115	265	0.44	0.0853	0.0034	0.4759	0.0212	0.0393	0.0006	1324	77.3	395	14.6	248	3.9
15K1-42	20	35	0.57	0.1358	0.0029	7.5260	0.2223	0.4002	0.0101	2174	37.3	2176	26.5	2170	46.3
15K1-43	358	825	0.43	0.0514	0.0012	0.2268	0.0049	0.0318	0.0003	257	49.1	208	4.0	202	1.9
15K1-44	89	228	0.39	0.1691	0.0023	9.2420	0.1605	0.3905	0.0048	2550	23.6	2362	16.0	2125	22.2
15K1-45	72	65	1.11	0.1082	0.0020	4.8627	0.1055	0.3227	0.0050	1770.1	35.3	1796	18.3	1803	24.1
15K1-46	170	188	0.90	0.0603	0.0020	0.4486	0.0137	0.0544	0.0009	613	72.2	376	9.6	341	5.5
15K1-47	421	426	0.99	0.0606	0.0017	0.4661	0.0122	0.0564	0.0011	633	61.1	389	8.4	354	6.8
15K1-48	206	452	0.46	0.0518	0.0015	0.2557	0.0073	0.0356	0.0005	276	64.8	231	5.9	225	3.2
15K1-49	192	420	0.46	0.0738	0.0013	1.6292	0.0346	0.1582	0.0024	1035	37.0	982	13.4	947	13.5
15K1-50	62	82	0.76	0.0705	0.0024	1.2980	0.0456	0.1343	0.0029	942.6	71.5	845	20.2	812	16.4
15K1-51	135	187	0.72	0.0596	0.0015	0.6950	0.0167	0.0840	0.0010	591	21.3	536	10.0	520	5.7
15K1-52	106	208	0.51	0.0724	0.0013	1.6226	0.0282	0.1611	0.0015	998	37.0	979	11.0	963	8.2
15K1-53	942	1287	0.73	0.0587	0.0012	0.2318	0.0046	0.0284	0.0003	567	38.0	212	3.8	180	2.1
15K1-54	41	73	0.56	0.0581	0.0027	0.5548	0.0246	0.0702	0.0014	532	101.8	448	16.1	438	8.2
15K1-55	84	276	0.30	0.1118	0.0018	3.8084	0.0746	0.2452	0.0039	1828.7	28.9	1595	15.8	1414	20.3
15K1-56	68	106	0.64	0.0713	0.0018	1.2444	0.0295	0.1270	0.0017	965	47.2	821	13.3	770	9.8
15K1-57	49	208	0.24	0.1462	0.0023	8.9498	0.1629	0.4378	0.0046	2302	26.4	2333	16.7	2341	20.6
15K1-58	136	516	0.26	0.1134	0.0016	4.9003	0.0893	0.3100	0.0044	1854	25.3	1802	15.4	1741	21.5
15K1-59	57	253	0.23	0.1129	0.0019	4.6705	0.0763	0.2972	0.0029	1846	29.5	1762	13.7	1677	14.3
15K1-60	268	645	0.41	0.0551	0.0014	0.2918	0.0073	0.0381	0.0004	416.7	54.6	260	5.7	241	2.7
15K1-61	265	278	0.95	0.0853	0.0038	0.5665	0.0291	0.0471	0.0010	1321	86.6	456	18.9	297	5.9
15K1-62	176	153	1.15	0.0801	0.0017	2.2632	0.0463	0.2044	0.0028	1198	36.1	1201	14.4	1199	14.7
15K1-63	159	347	0.46	0.0516	0.0015	0.3033	0.0086	0.0425	0.0005	265	66.7	269	6.7	268	3.4
15K1-64	163	610	0.27	0.1112	0.0015	4.3180	0.0572	0.2784	0.0020	1820	30.4	1697	11.0	1583	10.2
15K1-65	271	701	0.39	0.0526	0.0014	0.2571	0.0064	0.0353	0.0004	322.3	61.1	232	5.2	224	2.5
15K1-66	62	173	0.36	0.0639	0.0022	0.6468	0.0220	0.0741	0.0016	739	72.2	506	13.5	461	9.4

Table 1 Continued 2

Spot	w_B (10^{-6})		Th/U	Corrected isotope ratios						Isotope ages (Ma)					
	Th	U		$^{207}Pb/^{206}U$	1σ	$^{207}Pb/^{235}U$	1σ	$^{206}Pb/^{238}U$	1σ	$^{207}Pb/^{206}Pb$	1σ	$^{207}Pb/^{235}U$	1σ	$^{206}Pb/^{238}U$	1σ
15K1-67	1041	1092	0.95	0.0536	0.0012	0.2387	0.0050	0.0322	0.0003	354	84.3	217	4.1	204	1.9
15K1-68	519	1021	0.51	0.0545	0.0011	0.2398	0.0048	0.0318	0.0004	394	46.3	218	3.9	202	2.7
15K1-69	321	823	0.39	0.0546	0.0012	0.2570	0.0056	0.0339	0.0004	398	54.6	232	4.5	215	2.2
15K1-70	245	569	0.43	0.0536	0.0013	0.2437	0.0056	0.0329	0.0004	366.7	53.7	221	4.6	209	2.3
15K1-71	279	626	0.45	0.0558	0.0014	0.2632	0.0062	0.0342	0.0004	443	55.6	237	5.0	217	2.3
15K1-72	333	611	0.55	0.0536	0.0014	0.2393	0.0066	0.0324	0.0005	354	59.3	218	5.4	205	3.2
15K1-73	157	357	0.44	0.0498	0.0015	0.2595	0.0077	0.0381	0.0006	187	67.6	234	6.2	241	3.5
15K1-74	297	805	0.37	0.0531	0.0011	0.2364	0.0046	0.0323	0.0004	332	52.8	215	3.8	205	2.6
15K1-75	249	599	0.42	0.0529	0.0013	0.2422	0.0056	0.0332	0.0003	327.8	27.8	220	4.6	210	2.2
15K1-76	83	125	0.67	0.1074	0.0056	0.5247	0.0291	0.0358	0.0007	1755	96.3	428	19.4	227	4.6
15K1-77	525	704	0.75	0.0511	0.0012	0.2281	0.0055	0.0322	0.0003	256	55.5	209	4.6	204	2.2
15K1-78	160	283	0.56	0.0954	0.0058	0.6111	0.0420	0.0450	0.0007	1536	115.0	484	26.5	284	4.1
15K1-79	714	1259	0.57	0.0634	0.0013	0.3567	0.0119	0.0402	0.0008	720	44.4	310	8.9	254	5.2
15K1-80	193	402	0.48	0.0529	0.0015	0.2933	0.0082	0.0401	0.0005	324.1	66.7	261	6.5	254	3.1
15K1-81	210	317	0.66	0.0562	0.0015	0.4518	0.0130	0.0580	0.0008	461	26.9	379	9.1	363	5.1
15K1-82	303	176	1.72	0.0577	0.0015	0.6970	0.0174	0.0873	0.0009	517	59.3	537	10.4	539	5.5
15K1-83	72	674	0.11	0.1141	0.0016	4.4411	0.0622	0.2788	0.0023	1866	25.9	1720	11.7	1585	11.6
15K1-84	185	702	0.26	0.0562	0.0013	0.3996	0.0085	0.0512	0.0005	457	51.8	341	6.2	322	2.9
15K1-85	49	70	0.71	0.0617	0.0030	0.4951	0.0226	0.0594	0.0013	661.1	105.5	408	15.3	372	8.2
15K1-86	333	725	0.46	0.0542	0.0012	0.2445	0.0051	0.0324	0.0003	389	52.8	222	4.2	206	1.9
15K1-87	351	850	0.41	0.0536	0.0011	0.2608	0.0052	0.0351	0.0004	354	46.3	235	4.2	222	2.3
15K1-88	60	111	0.54	0.1490	0.0024	8.5607	0.1706	0.4125	0.0061	2344	28.4	2292	18.2	2226	28.0
15K1-89	107	311	0.34	0.1301	0.0021	6.9452	0.1158	0.3828	0.0035	2098	27.8	2104	14.9	2090	16.1
15K1-90	533	1106	0.48	0.0562	0.0014	0.2648	0.0064	0.0341	0.0004	457.5	27.8	238	5.1	216	2.7
15K1-91	139	161	0.86	0.0678	0.0017	1.1737	0.0282	0.1255	0.0018	865	50.5	788	13.2	762	10.2
15K1-92	152	379	0.40	0.0546	0.0013	0.3212	0.0080	0.0425	0.0006	394	56.5	283	6.1	268	4.0
15K1-93	101	171	0.59	0.0554	0.0021	0.3127	0.0117	0.0417	0.0009	428	85.2	276	9.1	263	5.5
15K1-94	781	1680	0.47	0.1117	0.0016	3.6461	0.0461	0.2359	0.0025	1828	21.1	1560	10.1	1365	13.0
15K1-95	121	891	0.14	0.1186	0.0017	4.1569	0.0664	0.2515	0.0029	1944.5	25.8	1666	13.1	1446	14.8
15K1-96	136	436	0.31	0.0808	0.0019	1.2213	0.0325	0.1095	0.0021	1217	47.1	810	14.8	670	12.1
15K1-97	21	61	0.34	0.1212	0.0102	1.4477	0.0882	0.0979	0.0044	1974	150.2	909	36.6	602	25.7
15K1-98	185	438	0.42	0.0681	0.0023	0.3859	0.0154	0.0416	0.0013	872	128.7	331	11.3	263	7.8
15K1-99	91	173	0.53	0.0898	0.0021	1.0522	0.0243	0.0848	0.0011	1421	44.9	730	12.0	525	6.3
15K1-100	379	1008	0.38	0.0620	0.0014	0.2796	0.0057	0.0326	0.0003	675.9	43.5	250	4.6	207	1.8
15K1-101	167	239	0.70	0.0575	0.0018	0.3937	0.0140	0.0497	0.0007	509	75.0	337	10.2	312	4.4
15K1-102	297	858	0.35	0.1273	0.0055	0.6351	0.0294	0.0353	0.0003	2061	75.8	499	18.3	224	2.1
15K1-103	142	404	0.35	0.0886	0.0014	2.7707	0.0681	0.2251	0.0048	1395	30.1	1348	18.4	1309	25.4
15K1-104	933	1204	0.77	0.0589	0.0013	0.2652	0.0059	0.0325	0.0004	565	46.3	239	4.7	206	2.8
15K1-105	186	533	0.35	0.0570	0.0018	0.2764	0.0077	0.0355	0.0005	500.0	73.1	248	6.1	225	3.3
15K1-106	615	639	0.96	0.1950	0.0025	8.8474	0.1183	0.3257	0.0029	2785	20.7	2322	12.3	1818	14.0
15K1-107	60	108	0.55	0.0748	0.0037	0.4012	0.0172	0.0404	0.0009	1063	98.9	343	12.4	255	5.6
15K1-108	65	94	0.68	0.1117	0.0022	5.2823	0.1037	0.3411	0.0041	1828	35.2	1866	16.8	1892	19.8
15K1-109	397	690	0.58	0.0553	0.0014	0.3080	0.0080	0.0401	0.0005	433	53.7	273	6.2	254	3.2
15K1-110	472	1167	0.40	0.0536	0.0011	0.2534	0.0047	0.0340	0.0003	366.7	44.4	229	3.8	216	1.8
15K1-111	199	192	1.03	0.1659	0.0023	10.3749	0.1559	0.4488	0.0044	2516	22.4	2469	14.0	2390	19.6
15K1-112	116	161	0.72	0.1044	0.0021	4.0593	0.1222	0.2741	0.0056	1706	32.4	1646	24.6	1561	28.1
15K1-113	294	538	0.55	0.1173	0.0017	4.9393	0.0983	0.3018	0.0046	1917	27.0	1809	16.9	1700	22.6
15K1-114	92	141	0.65	0.1230	0.0025	5.3105	0.1171	0.3113	0.0050	2067	35.6	1871	18.9	1747	24.4
15R2-1	747	901	0.83	0.0531	0.0016	0.2553	0.0103	0.0347	0.0008	332	66.7	231	8.3	220	4.9
15R2-2	899	672	1.34	0.1116	0.0044	0.5349	0.0263	0.0338	0.0006	1825	72.2	435	17.4	214	3.9
15R2-3	967	791	1.22	0.0607	0.0030	0.2930	0.0165	0.0348	0.0008	632	105.5	261	12.9	221	5.1
15R2-4	707	649	1.09	0.0483	0.0017	0.2348	0.0078	0.0348	0.0004	122	79.6	214	6.4	220	2.7
15R2-5	527	557	0.95	0.1011	0.0052	0.4903	0.0223	0.0350	0.0005	1656	96.1	405	15.2	222	3.1
15R2-6	573	497	1.15	0.0482	0.0017	0.2280	0.0069	0.0347	0.0005	109	78.7	209	5.7	220	3.0
15R2-7	672	874	0.77	0.0537	0.0018	0.2624	0.0108	0.0350	0.0007	367	77.8	237	8.7	222	4.2
15R2-8	859	748	1.15	0.0488	0.0018	0.2360	0.0093	0.0349	0.0006	139	89.8	215	7.7	221	3.6
15R2-9	757	546	1.39	0.0510	0.0017	0.2456	0.0081	0.0349	0.0004	243	77.8	223	6.6	221	2.7
15R2-10	1329	863	1.54	0.0512	0.0015	0.2496	0.0097	0.0349	0.0008	256	66.7	226	7.9	221	5.1
15R2-11	504	713	0.71	0.0551	0.0016	0.2651	0.0080	0.0348	0.0005	417	64.8	239	6.4	221	2.9
15R2-12	650	566	1.15	0.0554	0.0018	0.2714	0.0081	0.0356	0.0004	428	72.2	244	6.5	226	2.3
15R2-13	866	828	1.05	0.0592	0.0022	0.2850	0.0125	0.0346	0.0006	576	76.8	255	9.9	219	4.0
15R2-14	508	453	1.12	0.0504	0.0017	0.2485	0.0086	0.0349	0.0005	213	84.2	225	7.0	221	3.2
15R2-15	715	887	0.81	0.0528	0.0015	0.2557	0.0091	0.0347	0.0006	317	67.6	231	7.4	220	3.7
15R2-16	1133	955	1.19	0.0604	0.0017	0.2873	0.0083	0.0350	0.0007	620	56.5	256	6.5	221	4.1
15R2-17	598	370	1.62	0.0501	0.0021	0.2370	0.0084	0.0349	0.0005	198	99.1	216	6.9	221	3.2
15R2-18	768	686	1.12	0.0554	0.0017	0.2654	0.0080	0.0348	0.0004	428	65.7	239	6.4	221	2.5
15R2-19	919	1019	0.90	0.0506	0.0016	0.2420	0.0085	0.0344	0.0006	233	72.2	220	6.9	218	3.5
15R2-20	808	903	0.90	0.0519	0.0018	0.2523	0.0112	0.0346	0.0007	280	84.2	228	9.1	219	4.3

4 Analytical Results

4.1 Zircon U–Pb ages

Magmatic zircons are mostly colorless euhedral crystals, with short to long prismatic forms. However, detrital zircons are rounded to subrounded in shape, some displaying a core–rim texture (Fig. 5). These grains generally range in size from 50 to 150 μm with length/width ratios from 1:1 to 3:1. Most of the analyzed zircons exhibit typical oscillatory zoning in cathodoluminescence (CL) images, although some have inherited cores.

4.1.1 Sample 16R1-2 from Woruo Mountain

Seventeen zircon grains from sample 16R1-1 and twenty-seven from 16R1-2 were analyzed. Except for four discordant zircons, others for sample 16R1-1 are on or close to the concordia, but its age distribution is relatively diffuse (Fig. 6a). This tuffite yields only 17 zircons, one of which is Late Triassic in age. Therefore, the youngest individual zircon age is 226±2.7 Ma, which can be interpreted as the maximum depositional age of sample 16R1-1. All analyzed spots of sample 16R1-2 were concordant, and define a narrow age range between 203 and 220 Ma. Twenty-seven grains give a totally weighted mean $^{206}Pb/^{238}U$ age of 209.9±1.7 Ma for sample 16R1-2, and the two youngest grains give a weighted mean $^{206}Pb/^{238}U$ age of 203±3.6 Ma (Fig. 6b).

4.1.2 Sample 15R2 from the Dongqu River

Twenty U-Pb spots were analysed on 20 zircon grains for sample 15R2, for which 18 analyses were concordant. All analysed zircons exhibit clear oscillatory magmatic zoning in CL images with Th/U ratios of 0.64–1.62 (Fig. 5; Table 1), suggesting an entirely magmatic origin. A population of 18 concordant grains give a range from 214 Ma to 226 Ma and yield a weighted mean $^{206}Pb/^{238}U$ age of 221.1±1.5 Ma (MSWD=0.31, Fig. 6c), which is consistent with sample 15R1 and published data from the east of the North Qiangtang depression (Fu et al., 2010a).

4.1.3 Samples 15R1 and 15K1 from Quem Co

Thirty U-Pb spots were analysed on 30 zircon grains for sample 15R1, for which 26 analyses were concordant. The concordant ages range from 211 Ma to 781 Ma, but the majority fall in clusters of 211–239 Ma and 311–345 Ma (Fig. 6d). The predominant population of 17 concordant grains yield a weighted mean $^{206}Pb/^{238}U$ age of 221.5±2.6 Ma (excluding 239 Ma), and a subpopulation of 5 concordant grains yield a weighted mean $^{206}Pb/^{238}U$ age of 318.4 ± 5.3 Ma (excluding 345 Ma), respectively. A total of one hundred and fourteen U-Pb spots were analysed on 114 zircon grains for sample 15K1. Excluding 11 discordant zircons, the concordant ages range from 201 Ma ($^{206}Pb/^{238}U$ age < 1000 Ma) to 2499 Ma ($^{207}Pb/^{206}U$ age > 1000 Ma), with a maximum cluster of 201.5–225

Table 2 In-situ Hf isotopic data for zircon grains from the North Qiangtang depression, Tibet

Spot	$^{176}Hf/^{177}Hf$	$^{176}Lu/^{177}Hf$	$^{176}Yb/^{177}Hf$	$\varepsilon_{Hf}(0)$	$\varepsilon_{Hf}(t)$	T_{DM}	T_{DM}^c	fLu/Hf	Spot	$^{176}Hf/^{177}Hf$	$^{176}Lu/^{177}Hf$	$^{176}Yb/^{177}Hf$	$\varepsilon_{Hf}(0)$	$\varepsilon_{Hf}(t)$	T_{DM}	T_{DM}^c	fLu/Hf
16R1-1	0.282510	0.000752	0.024652	−9.3	−4.9	1042	1381	−0.98	15K1-06	0.282784	0.000965	0.025224	0.4	4.9	662	841	−0.97
16R1-3	0.282471	0.000660	0.023759	−10.6	−6.0	1094	1453	−0.98	15K1-07	0.282729	0.002759	0.074409	−1.5	2.9	777	960	−0.92
16R1-4	0.282478	0.000850	0.030345	−10.4	−5.8	1090	1441	−0.97	15K1-08	0.282722	0.001652	0.042889	−1.8	2.8	765	966	−0.95
16R1-6	0.282430	0.000557	0.018967	−12.1	−7.4	1148	1531	−0.98	15K1-09	0.282716	0.001270	0.031516	−2.0	2.5	764	978	−0.96
16R1-8	0.282469	0.000584	0.020471	−10.7	−6.2	1095	1460	−0.98	15K1-10	0.282637	0.001310	0.034931	−4.8	0.0	878	1128	−0.96
16R1-11	0.282321	0.001195	0.040127	-16.0	−11.4	1321	1751	−0.96	15K1-11	0.282779	0.002123	0.055578	0.2	4.5	691	862	−0.94
16R1-13	0.282495	0.001462	0.050698	−9.8	−5.4	1084	1414	−0.96	15K1-12	0.282754	0.001846	0.049480	−0.6	3.6	722	911	−0.94
16R1-15	0.282470	0.000731	0.025186	−10.7	−6.2	1097	1458	−0.98	15K1-13	0.282699	0.001785	0.049267	−2.6	1.9	800	1014	−0.95
16R1-16	0.282186	0.000993	0.035329	−20.7	−16.0	1502	2009	−0.97	15K1-14	0.282703	0.001544	0.041254	−2.4	2.1	788	1004	−0.95
16R1-17	0.282439	0.001202	0.044254	−11.8	−7.3	1155	1521	−0.96	15K1-15	0.282703	0.001581	0.042737	−2.4	2.2	789	1001	−0.95
16R1-18	0.282354	0.000576	0.018311	−14.8	−10.2	1254	1681	−0.98	15K1-16	0.282691	0.001910	0.049780	−2.9	1.5	815	1032	−0.94
16R1-19	0.282327	0.000735	0.028694	−15.7	−11.1	1296	1733	−0.98	15K1-17	0.282710	0.002441	0.065754	−2.2	2.0	798	999	−0.93
16R1-20	0.282486	0.000764	0.029925	−10.1	−-5.7	1077	1428	−0.98	15K1-18	0.282665	0.001682	0.039853	−3.8	0.9	846	1077	−0.95
16R1-22	0.282465	0.000700	0.023115	−10.9	−6.4	1104	1468	−0.98	15K1-19	0.282675	0.001462	0.038045	−3.4	1.3	827	1055	−0.96
16R1-23	0.282405	0.000826	0.029058	−13.0	−8.5	1191	1585	−0.98	15R2-01	0.282434	0.002609	0.070500	−11.9	−7.5	1207	1538	−0.92
16R1-25	0.282454	0.000620	0.022408	−11.2	−6.9	1117	1491	−0.98	15R2-03	0.282338	0.002302	0.063022	−15.3	−10.9	1336	1724	−0.93
16R1-26	0.282378	0.000922	0.030578	−13.9	−9.5	1232	1639	−0.97	15R2-04	0.282475	0.002215	0.059708	−10.5	−6.0	1136	1456	−0.93
15R1-02	0.282581	0.000709	0.016993	−6.8	−2.0	943	1236	−0.98	15R2-08	0.282380	0.001869	0.049015	−13.9	−9.3	1261	1638	−0.94
15R1-03	0.282365	0.002167	0.056095	−14.4	−9.8	1292	1668	−0.93	15R2-09	0.282414	0.001895	0.051724	−12.7	−8.1	1213	1571	−0.94
15R1-13	0.282573	0.002095	0.051801	−7.0	−2.5	989	1261	−0.94	15R2-10	0.282422	0.002099	0.056524	−12.4	−7.8	1207	1556	−0.94
15R1-14	0.282625	0.001091	0.025937	−5.2	−0.7	889	1155	−0.97	15R2-11	0.282409	0.001343	0.035875	−12.8	−8.2	1202	1577	−0.96
15R1-15	0.282521	0.001908	0.050566	−8.9	−4.6	1060	1367	−0.94	15R2-12	0.282433	0.002800	0.076851	−12.0	−7.5	1215	1541	−0.92
15R1-23	0.282598	0.001821	0.045592	−6.1	−1.6	946	1210	−0.95	15R2-13	0.282276	0.001946	0.052773	−17.5	−13.0	1412	1840	−0.94
15R1-27	0.282569	0.001869	0.046515	−7.2	−2.6	989	1267	−0.94	15R2-14	0.282412	0.002101	0.056410	−12.7	−8.2	1223	1578	−0.94
15R1-30	0.282575	0.002245	0.056367	−7.0	−2.4	990	1258	−0.93	15R2-15	0.282403	0.002073	0.056063	−13.0	−8.5	1234	1595	−0.94
15K1-01	0.282663	0.000987	0.024688	−3.9	0.7	834	1079	−0.97	15R2-16	0.282386	0.001807	0.047606	−13.7	−9.1	1250	1625	−0.95
15K1-02	0.282764	0.002091	0.055818	−0.3	4.3	713	887	−0.94	15R2-17	0.282444	0.001934	0.051392	−11.6	−7.0	1171	1513	−0.94
15K1-03	0.282703	0.001068	0.028438	−2.4	2.1	779	1001	−0.97	15R2-18	0.282416	0.001909	0.050995	−12.6	−8.0	1211	1569	−0.94
15K1-04	0.282698	0.001774	0.046040	−2.6	1.8	802	1016	−0.95	15R2-19	0.282429	0.001559	0.040212	−12.1	−7.5	1180	1539	−0.95
15K1-05	0.282715	0.000912	0.022823	−2.0	2.7	759	974	−0.97	15R2-20	0.282360	0.001224	0.032633	−14.6	−9.9	1267	1671	−0.96

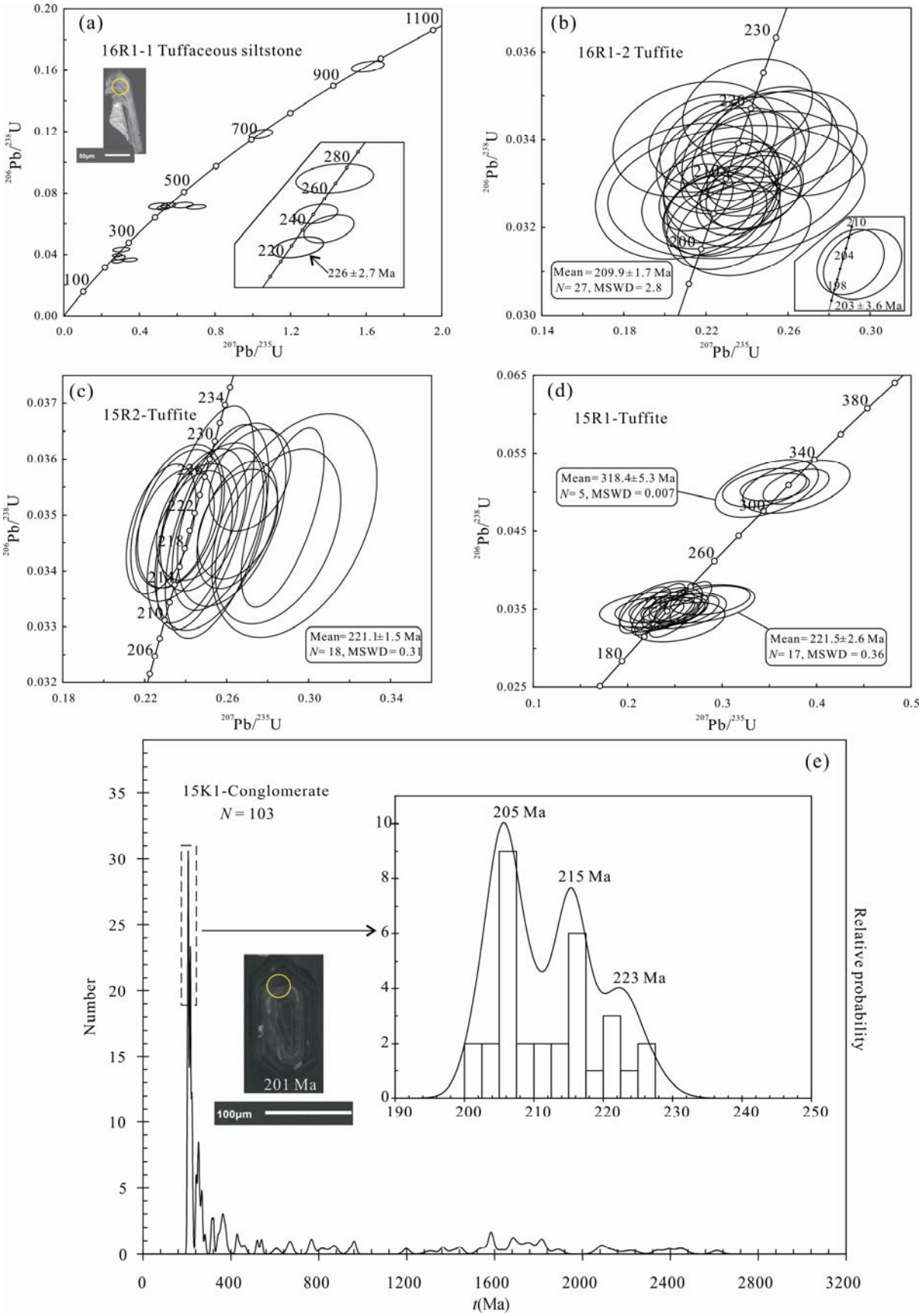

Fig. 6. Zircon U–Pb concordia diagrams (a–d) with frequency distribution histogram (e).

Ma (n=32, Fig. 6e). The cluster, based on 32 analyzed zircons from sample 15K1, shows that there are three major peaks at ca. 205 Ma (n=15), ca. 215 Ma (n=11) and ca.223 Ma (n=6, Fig. 7e), probably corresponding to the three episodes of the Nadigangri phase.

4.2 Zircon Lu-Hf isotopes

4.2.1 Sample 16R1-2 from Woruo Mountain

In situ Lu-Hf isotopic analyses of the zircons were carried out on a total of 17 dated zircons from sample 16R1-2, guided by CL images (Fig. 5). The analyses yielded variable $^{176}Hf/^{177}Hf$ ratios between 0.282186 and 0.282510 with a relatively wide range of $\varepsilon_{Hf}(t)$ values from -11.4 to -4.9. Apart from one zircon with age of 2.01 Ga, the T_{DM2}(Hf) model ages range from 1.38 Ga to 1.75 Ga (Table 2).

4.2.2 Samples 15R1 and 15K1 from Quem Co

8 spot analyses of zircons from sample 15R1 yield $^{176}Hf/^{177}Hf$ ratios from 0.282365 to 0.282625 and negative $\varepsilon_{Hf}(t)$ values from -0.7 to -9.8 with T_{DM2}(Hf) model ages ranging from 1.16 to 1.67 Ga. In total, 19 detrital zircon grains of the maximum cluster from sample 15K1 yield relatively high $^{176}Hf/^{177}Hf$ ratios between 0.282637 and 0.282784 and positive $\varepsilon_{Hf}(t)$ values from +0.1 to +4.9. Corresponding T_{DM2}(Hf) model ages of these zircons vary from 1.13 to 0.84 Ga.

4.2.3 Sample 15R2 from Dongqu River

16 zircon grains from the sample 15R2 were analyzed for *in situ* Lu-Hf isotopic composition. All analyses of zircons exhibited variable $^{176}Hf/^{177}Hf$ ratios between 0.282267 and 0.282475, equivalent to initial $\varepsilon_{Hf}(t)$ values from -13.0 to -6.0. Corresponding T_{DM2}(Hf) model ages of these zircons vary from 1.84 to 1.46 Ga with a dominant model age of 1.55 Ga.

5 Discussion

5.1 Temporal range of the Nadigangri Formation

The Nadigangri Formation had been assigned to an Early Jurassic stratigraphic sequence of the Yanshiping Group (Zhao Zhengzhang et al., 2001), until Wang Jian et al. (2007b) reset it to the Late Triassic through precise SHRIMP U-Pb dating and rock associations. In order to establish the temporal framework of the Nadigangri Formation, we have collected the published ages of the Late Triassic rocks scattered throughout the three rift troughs of the Qiangtang Basin, as follows: the dacite and dacitic tuffite in the Juhua Mountain area, gave zircon U-Pb ages of 217 and 225 Ma, respectively (Zhai Qingguo and Li Cai, 2007; Fu Xiugen et al., 2008). Zircon SHRIMP U-Pb ages of dacite, rhyolitic lava and tuffite in the Shishui River, Nadigangri and Woruo Mountain regions have been dated at 208, 205, 210, 215 and 216 Ma, respectively (Wang Jian et al., 2007b, 2008; Li Xueren et al., 2018b). Bai Yunshan et al. (2005) and Fu et al. (2010a) obtained zircon U-Pb ages of 212 and 220 Ma from rhyolite and basalt at Geladandong Snow Mountain. The basalts of Wanwanliang, Jiaomuchaka, Xiaochaka and Biluo Co yield whole rock Ar-Ar and zircon U-Pb ages of 202, 206, 223 and 202 Ma respectively (Zhu Tongxing et al., 2012a, 2012b; Fu et al. 2016b). As mentioned above, these ages were mostly obtained from scattered lavas in

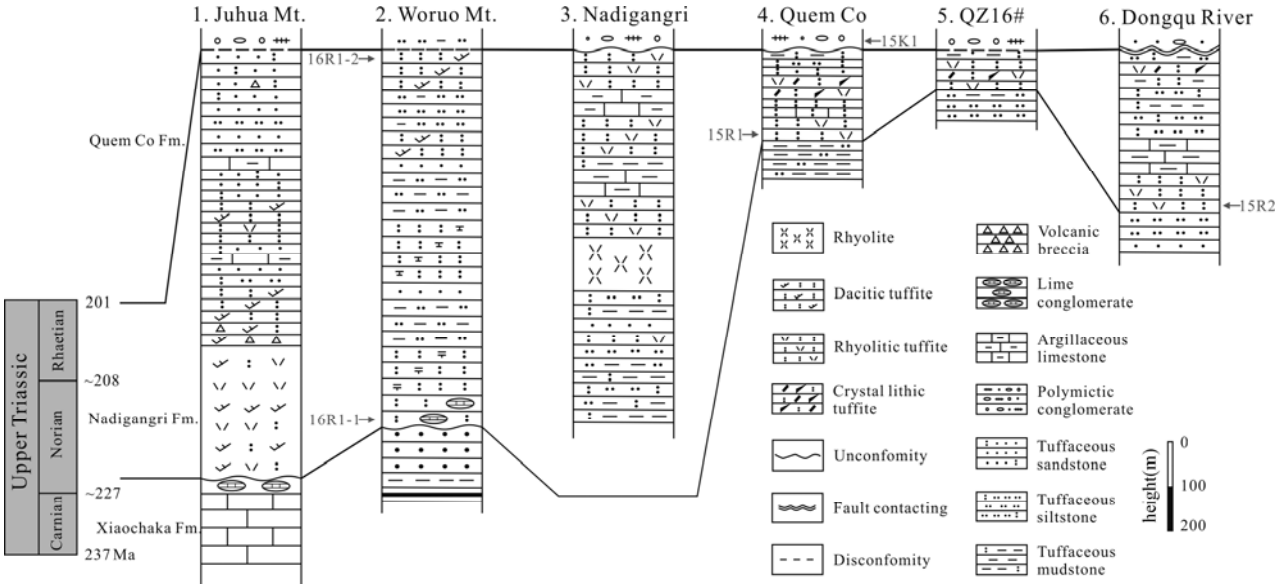

Fig. 7. Lithological columns of representative profiles of the Late Triassic sedimentary successions of the Nadigangri Formation in the North Qiangtang depression, Tibet (modified after Fu et al. (2010b), QZ16 well and this study).
Red letters represent the location of samples taken.

different parts of the basin. Obviously, the temporal range cannot be well constrained due to poor outcrops and the lack of volcanic successions. However, the coeval sedimentary successions with tuffite interlayers will provide a more reliable constraint on the temporal range of the volcano-sedimentary succession during the Late Triassic.

The youngest grains of sample 16R1-1 and 16R1-2 from the top and bottom of the Woruo Mountain section give respective $^{206}Pb/^{238}U$ ages of 226 and 203 Ma. The Xiaochaka Formation is composed of lithic quartz sandstone intercalated with mudstone, fossils of which were dated as Carnian to Norian (Feng Xinglei et al., 2010). It is unconformably overlain by sedimentary successions of the Nadigangri Formation. The lowermost part of the Nadigangri Formation comprises tuffaceous siltstone including limestone breccia, the youngest magmatic zircon of which yields a $^{206}Pb/^{238}U$ age of 226 Ma. This result is relatively consistent with the previously published $^{206}Pb/^{238}U$ age of 225 Ma, obtained from the lowermost part of the Nadigangri Formation, underlain unconformably by the paleo-weathered crust of Juhua Mountain (Zhu Tongxing et al., 2002; Fu Xiugen et al., 2008). The uppermost tuffite layer yields a weighted mean $^{206}Pb/^{238}U$ age of 203 Ma. Therefore, we interpret 226 and 203 Ma as the maximum and minimum depositional age at the bottom and top of the Nadigangri Formation at Woruo Mountain, respectively.

The Late Triassic Nadigangri successions of the Quem Co depression are composed largely of green tuffite with a thickness of ca. 200 m (Fig. 7). It is conformably underlain by the Bagong (Xiaochaka) Formation and unconformably overlain by the Quem Co Formation, the lowermost part of which gives a concordant U-Pb zircon age of 221.5 Ma in the Late Triassic Norian. It is noted that there is another concordant age of 318.4 Ma that may be associated with a magmatic event occurring in the Late Carboniferous. In addition, the Late Triassic age is consistent with the age of 221.1 Ma from the Dongqu River section, as well as the age of 220.4 Ma from Geladandong adjacent to Quem Co (Fu et al., 2010a). According to the latest geological survey, large volumes of basaltic rocks are exposed in the Tuotuo River area, the ages of which range from 203 to 220 Ma (Fig. 1b; Wang et al., 2008; Duan Qifa et al., 2013; Deng Zhonglin et al., 2014; Song et al., 2015; Li Xueren et al., 2018a). Here, we interpret 221 Ma as the best estimation of the maximum depositional age of the Nadigangri Formation in the east of the North Qiangtang depression. We also provide available constraints on the upper age of the Nadigangri successions, using detrital zircon ages from the conglomerate of the Quem Co Formation. In this connection, we selected all sorts of single gravel covering sedimentary, metamorphic and volcanic materials from the bottom of the Quem Co Formation. The frequency distribution histogram shows that the Late Triassic rocks were a significant source of sediment for the conglomerate of the Quem Co Formation (Fig. 6e). Detrital zircon analyses not only allowed us to resolve the original sources of the conglomerate, but also provided certain constraints on the depositional age of the Quem Co Formation, as well as on the upper limit of the Nadigangri Formation. The youngest zircons U-Pb age populations of the Late Triassic cluster yield weighted mean ages of ca. 205 Ma, ca. 215 Ma and ca. 223 Ma, respectively (Fig. 6e). Furthermore, the youngest zircon U-Pb age is 201.5 Ma and the oldest 225 Ma of the Late Triassic cluster. Therefore, the depositional age of the Quem Co Formation is younger than 201.5 Ma, which is consistent with the regional stratigraphic sequence (Fu Xiugen et al., 2010c). Previous studies only assigned the Quem Co Formation to the Middle Jurassic (Hao Ziwen and Rao Rongbiao, 2009), until Wang Jian et al. (2009) revised it to the Early Jurassic through the stratigraphic relationship between the Quem Co Formation and the Nadigangri Formation. This paper once again demonstrates that the Quem Co Formation has the characteristics of diachronism from the Early to the Middle Jurassic via detrital zircons. In other words, the Nadigangri phase is earlier than 201.5 Ma and may be later than 225 Ma.

As discussed above, the Late Triassic Nadigangri phase reasonably ranges from 201 to 225 Ma in the North Qiangtang depression, which is somewhat broader than the previously defined range (205 to 220 Ma; Fu et al., 2010a).

5.2 Three main episodes of the Nadigangri phase

We have come to the conclusion that the Nadigangri phase extends from the Norian to the Rhaetian of the Late Triassic (201 to 225 Ma). Based on our data, coupled with the eruption ages of coeval lavas, we found that there are three relatively concentrated age groups, i.e., 201–205 Ma, 210–217 Ma and 220–225 Ma, respectively. The temporal range from 201 to 205 Ma includes 201.5 Ma and 203 Ma (this study; Song et al., 2015), 201.8 Ma for basalt from Biluo Co (Fu et al., 2016b), 205 Ma for rhyolite from Nadigangri (Wang Jian et al., 2007b). The age group from 210 to 217 Ma has 210 Ma, 215 Ma and 217 Ma for rhyolite from Nadigangri and the Shengli River (Wang Jian et al., 2007b; Zhai et al., 2013; Li Xueren et al., 2018b), 212 Ma for rhyolite from Geladandong (Bai Yunshan et al., 2005), 216 Ma of trachybasalt from Tuotuohe (Li Xueren and Wang Jian, 2018a) and 216 Ma of tuffite from Woruo Mountain (Wang et al., 2008). The

age range from 220 to 225 Ma contains 219, 220, 223, 225 and 226 Ma (Zhai Qingguo and Li Cai, 2007; Wang et al., 2008; Fu et al., 2010a; Duan Qifa et al. 2013; this study). Furthermore, the three age groups coincide with the detrital zircon ages of the Late Triassic cluster of the Quem Co conglomerate (Fig. 6e).

More importantly, the exposure of the Nadigangri Formation matches well with the rifting basement of the Upper Triassic strata, which indicates that the volcanic-sedimentary event was a localized event related to rifting in the region (Fig. 1b). Therefore, we interpret the three age groups as the initial rifting episode, the further rifting episode and the final rifting episode from early to late by ages, respectively. In the first episode, the initiation of a continental extensional setting was triggered by the opening of the Bangong–Nujiang Tethyan Ocean, and the rock association consists mainly of a large amount of basic lavas exposed in Geladandong, Wanwanliang and Xiaochaka. Sequentially, a more intense rifting has occurred here, when a series of horst-graben structures with a NW–SE trend was formed, as well as a great quantity of felsic lavas along these structures in the three rift troughs (Tan Fuwen et al., 2016). During the final episode, the pattern of the North Qiangtang depression had been preliminarily formed and only minor basic and felsic lavas were erupted. In fact, volcanic eruption of the Nadigangri phase was a continuous process without a gap, but it was multi-point and on different scales in different regions. It should be noted that volcanic tuff occurs throughout the Nadigangri Formation. The latest geological survey of the Qiangtang oil and gas team shows that a complete section that recorded the transition from foreland basin to rift basin in the North Qiangtang depression, gave zircon U-Pb ages of 206 Ma, 216 Ma and 227 Ma, corresponding to the three main eruption-sedimentary cycles, respectively. The three rifting episodes are consistent with the Late Triassic rifting mechanism and the volcanic-sedimentary event in the North Qiangtang depression (Li Xueren et al., 2018b; Wang Jian and Fu Xiugen, 2018).

5.3 Constraints on provenance of the Nadigangri rocks

A total of 60 Hf isotopic analyses were obtained from magmatic and detrital zircons dated in the Nadigangri Formation. The results show that all analyses of magmatic zircons from felsic tuffite plot below the CHUR line, whereas all others of detrital zircons from conglomerate plot between the depleted mantle and CHUR lines (Fig. 8), indicating that the Late Triassic source rocks were probably at least partly derived from recycled crust with a model age of 1.5–1.8Ga and juvenile mantle-derived melts with a model age of ca. 1.1 Ga, respectively. According to T_{DM2}(Hf) model ages (Fig. 8), it appears that the source region likely underwent two major episodes of crustal growth at 1.8 Ga and 1.5 Ga, responding to the metamorphic basement and the crystalline basement, respectively (Huang Jijun, 2001; Deng Xiguang et al., 2007; Tan Fuwen et al., 2009).

The source rocks of detrital zircons were almost entirely igneous, based on the magmatic growth zoning as imaged by CL and the Th/U ratios (Fig. 7e; Table 1). In addition, the provenance of the conglomerate shows the characteristics of the proximal source. Hence, we propose that the source rocks are roughly derived from the felsic rocks that had been exposed to erosion in the Nadigangri phase. This indicates that there were probably two types of felsic rocks with different source region characteristics in the Late Triassic. It is generally accepted that the onset of the Qiangtang Mesozoic rift basin was a synchronous process with the closure of the KJSZ in the north and the opening of the Bangong–Nujiang Tethyan Ocean in the south. These complex characteristics are consistent with the tectonic evolution of the Qiangtang Basin.

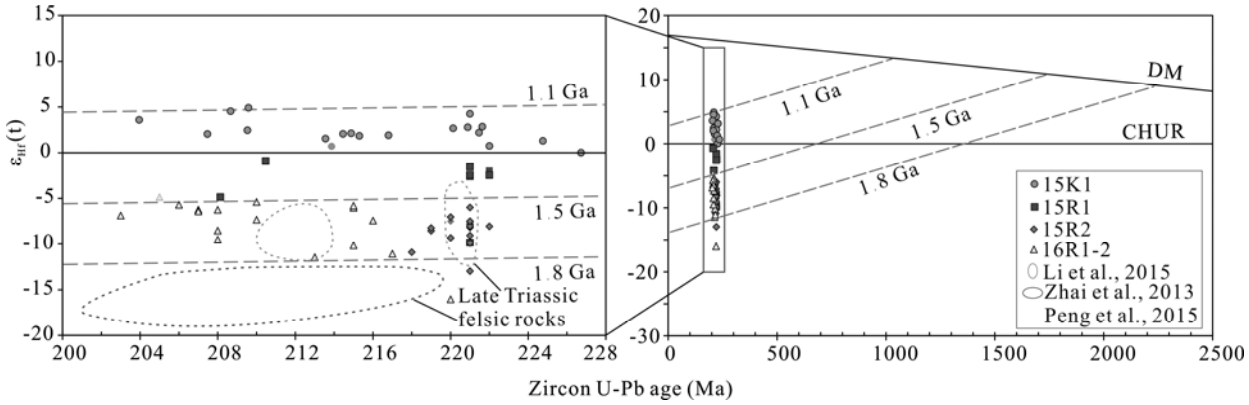

Fig. 8. Relationship between $\varepsilon_{Hf}(t)$ values and U-Pb ages for zircons from the tuffite and conglomerate in the Woruo Mountain, Quem Co and Dongqu River areas, and published data.

Hf isotopic compositions of chondrite and depleted mantle are from Blichert-Toft and Albarede (1997) and Vervoort and Blichert-Toft (1999).

6 Conclusions

Geochronological and Hf isotopic data from magmatic and detrital zircons for the Late Triassic rocks of the Nadigangri Formation in the North Qiangtang depression, Tibet, allow us to reach the following conclusions:

(1) The late Triassic Nadigangri phase ranges from 201 to 225 Ma, which can be subdivided into three major episodes of 201–205 Ma, 210–217 Ma and 220–225 Ma in terms of magmatic and detrital zircon ages from the sedimentary succession of the Nadigangri Formation.

(2) Hf isotopic data suggests that the felsic tuffite originated from partial melting of the Mesoproterozoic crustal basement and the source rock of the detrital zircons derived from partial melting of the Neoproterozoic juvenile mantle-derived crust, indicating that the volcanic rocks of the Nadigangri Formation have relatively complex source characteristics.

Acknowledgements

We thank Professor Zhaochu Hu for helping with the LA-ICP-MS U-Pb and Hf analyses. We would also like to express our appreciation to all members of the project team from the Chengdu Center of the Chinese Geological Survey, for their support and assistance during the fieldwork stage of the study. This study was jointly funded by the National Natural Science Foundation of China (Grant No. 41502112 and 41702119) and a project program under China Geological Survey (No. DD20160159).

Manuscript received Apr. 7, 2017
accepted Jan. 15, 2018
edited by Fei Hongcai

References

Bai Yunshan, Li Li, Niu Zhijun and Cui Jiangli, 2005. Characteristics and tectonic setting of Eerlongba Formation volcanic rocks in Galadaindong area of central Qiangtang. *Acta Geoscientica Sinica*, 26(2): 113–120 (in Chinese with English abstract).

Blichert-Toft, J. and Albarède, F., 1997. The Lu-Hf isotope geochemistry of chondrites and the evolution of the mantle-crust system. *Earth and Planetary Science Letters*, 154(1–4): 243–258.

Chen Wenxi, Wang Jian, Wang Zhengjiang and Fu Xiugen, 2007. Discovery and Significance of Paleokarst Unconformity between the Xiaochaka Formation and the Nadigangri Formation in Juhuashan Region, Qiangtang Basin, Northern Xizang (Tibet). *Geological Review*, 53(5): 699–703 (in Chinese with English abstract).

Deng Xiguang, Zhang Jinjiang, Zhang Yuquan and Liu Dunyi, 2007. SHRIMP U-Pb dating of zircons from blueschist in the central part of the Qiangtang block, northern Tibet, China, and its implications. *Geological Bulletin of China*, 26(6): 698–702 (in Chinese with English abstract).

Duan Qifa, Niu Zhijun and Wang Jianxiong, 2013. *Regional Geological Report of Zhigengaka Sheet (1:250000)*. Wuhan: China University of Geosciences Press, 1–286 (in Chinese).

Deng Zhonglin, An Yongsheng and Wang Qinghai, 2014. *Regional Geological Report of Tuotuo River Sheet (1:250000)*. Wuhan: China University of Geosciences Press, 1 –269 (in Chinese).

Feng Xinglei, Fu Xiugen, Tan Fuwen and Chen Wenbin, 2010. Geochemical Characteristics and Tectonic Significance of Upper Triassic Tumengela Formation in Woruo Mountains, North Qiangtang Basin. *Geoscience*, 24(5): 910–918 (in Chinese with English abstract).

Fu Xiugen, Wang Jian., Wang Zhengjiang and Chen Wenxi, 2008. U-Pb Zircon Age and Geochemical Characteristics of Volcanic Rocks from the Juhua Mountain Area in the northern Qiangtang Basin, northern Tibet . *Geological Review*, 54(2): 232–242 (in Chinese with English abstract).

Fu Xiugen, Wang Jian, Wu Tao and He Jianglin, 2009. Discovery of the large-scale paleo–weathering crust in the Qiangtang basin, northern Tibet, China and its significance. *Geological Bulletin of China*, 28(6): 696–700 (in Chinese with English abstract).

Fu, X.G., Wang, J., Tan, F.W., Chen, M., and Chen, W.B., 2010a. The Late Triassic rift-related volcanic rocks from eastern Qiangtang, northern Tibet (China): age and tectonic implications. *Gondwana Research*, 17: 135–144.

Fu Xiugen, Wang Jian, Chen Wenbin and Feng Xinglei, 2010b. Age and tectonic implications of the Late Triassic Nadi Kangri volcanic rocks in the Qiangtang basin, northern Tibet, China. *Journal of Chengdu University of Technology*, 37(6): 605–615 (in Chinese with English abstract).

Fu Xiugen, Wang Jian, Wu Tao and He Jianglin, 2010c. Stratigraphy and paleoenvironment of the Quemo Co formation in Shengli river area, northern Tibet. *Geology in China*, 37(5): 1305–1312 (in Chinese with English abstract).

Fu, X.G., Wang, J., Tan, F.W., Chen, M., Li, Z.X., Zeng, Y.H., and Feng, X.L., 2016a. New insights about petroleum geology and exploration of Qiangtang Basin, northern Tibet, China: A model for low-degree exploration. *Marine and Petroleum Geology*, 77: 323–340.

Fu, X.G, Wang, J., Feng, X.L. Wang, D., Chen, W.B., Song, C.Y., and Zeng, S.Q., 2016b. Early Jurassic carbon-isotope excursion in the Qiangtang Basin (Tibet), the eastern Tethys: Implications for the Toarcian Oceanic anoxic event. *Chemical Geology*, 442: 62–72.

Griffin, W.L., Pearson, N.J., Belousova, E., Jackson, S.E., Achterbergh, E.V., O'Reilly, S.Y., and Shee, S.R., 2000. The Hf isotope composition of cratonic mantle: LAM-MC-ICPMS analysis of zircon megacrysts in kimberlites. *Geochimica et Cosmochimica Acta*, 64(1): 133–147.

Hao Ziwen and Rao Rongbiao, 2009. *Multiple Classification and Correlation of the Stratigraphy of China: Regioml Stratigraphy of Southwest China*. Wuhan: China University of Geosciences Press, 120–126 (in Chinese).

Hu, Z.C., Liu, Y., Gao, S., Liu, W., Zhang, W., Tong, X., Lin, L., Zong, K., Li, M., and Chen, H., 2012. Improved in situ Hf isotope ratio analysis of zircon using newly designed X skimmer cone and jet sample cone in combination with the addition of nitrogen by laser ablation multiple collector ICP–

MS. *Journal of Analytical Atomic Spectrometry*, 27(9): 1391–1399.

Huang Jijun, 2001. Structural Characteristics of the Basement of the Qiangtang Basin. *Acta Geologica Sinica*, 75(3): 333–337 (in Chinese with English abstract).

Kapp, P., Yin, A., Manning, C.E., Harrison, T.K., Taylor, M.H., and Ding, L., 2003. Tectonic evolution of the early Mesozoic blueschist–bearing Qiangtang metermorphic belt, central Tibet. *Tectonics*, 22(4): 17.

Li, G.M., Li, J.X., Zhao, J.X., Qin, K.Z., Cao, M.J., and Evans, J., 2015. Petrogenesis and tectonic setting of Triassic granitoids in the Qiangtang terrane, central Tibet: Evidence from U-Pb ages, petrochemistry and Sr-Nd-Hf isotopes. *Journal of Asian Earth Sciences*, 105: 443–455.

Li Xueren and Wang Jian, 2018a. New evidence for the Late Triassic syn-rifting in the eastern of North Qiangtang depression: redefining of the stratigraphic age of volcanic rocks and conglomerates from the Jiapila Formation. *Earth Science Frontiers*, https://doi.org/10.13745/j.esf.sf.2018.5.25.

Li Xueren, Wang Jian and Wan Youli, 2018b. The late Triassic rifted evolution of Qiangtang basin: Evidence from the syn-rifting Nadigangri Formation. *Journal of Northeast Petroleum University*, 42(2): 23–3 (in Chinese with English abstract).

Liu, Y.S., Hu, Z.C., Gao, S., Günther, D., Xu, J., Gao, C.G., and Chen, H.H., 2008. In situ analysis of major and trace elements of anhydrous minerals by LA-ICP-MS without applying an internal standard. *Chemical Geology*, 257: 34–43.

Liu, Y.S., Gao, S., Hu, Z.C., Gao, C.G., Zong, K.Q., and Wang, D.B., 2010. Continental and oceanic crust recycling-induced melt-peridotite interactions in the Trans-North China Orogen: U-Pb dating, Hf isotopes and trace elements in zircons of mantle xenoliths. *Journal of Petroleum*, 55(15): 1535–1546.

Ludwig, K.R., 2012. ISOPLOT 3.75: A Geochronological Toolkit for Microsoft Excel. Berkeley: *Geochronology Center Special Publication*, 1–71.

Morel, M.L.A., Nebel, O., Nebel-Jacobsen, Y.J., Miller, J.S., and Vroon, P.Z., 2008. Hafnium isotope characterization of the GJ -1 zircon reference material by solution and laser-ablation MC -ICPMS. *Chemical Geology*, 255(1–2): 231–235.

Peng, T.P, Zhao, G.C., Fan, W.M., Peng, B.X., and Mao, Y.S., 2015. Late Triassic granitic magmatism in the Eastern Qiangtang, Eastern Tibetan Plateau: Geochronology, petrogenesis and implications for the tectonic evolution of the Paleo-Tethys. *Gondwana Research*, 27(4): 1494–1508.

Pearce, J.A., and Mei, H., 1988. Volcanic Rocks of the 1985 Tibet Geotraverse: Lhasa to Golmud. *Philosophical Transactions of the Royal Society of London*, 327(1594): 169–201.

Perkins, M.E., and Nash, B.P., 2002. Explosive silicic volcanism of the Yellowstone hotspot: The ash fall tuff record. *Geological Society of America Bulletin*, 114(3): 367–381.

Song, C.H., Zeng, Y.Y., Yan, M.D., Fang, H.M., Pan, J.Q., Liu, X.F., Meng, Q.Q, Hu, C.H., and Zhong, S.R., 2017. Sedimentary Conditions of Evaporites in the Late Jurassic Xiali Formation,Qiangtang Basin:Evidence from Geochemistry Records. *Acta Geologica Sinica* (English Edition), 91(1): 156–174.

Spikings, R., Reitsma, M.J., Boekhout, F., Mišković, A., Ulianov, A., Chiaradia, M., Gerdes, A., and Schaltegger, U., 2016. Characterization of Triassic Rifting in Peru and implications for the early disassembly of western Pangaea. *Gondwana Research*, 114(3): 367–381.

Tan Fuwen, Wang Jian, Fu Xiugen Chen Ming and Du Bowei, 2009. U-Pb zircon SHRIMP age of metamorphic rocks from the basement of the qiangtang basin, northern Tibet, and its geological significance. *Acta Petrologica Sinica*, 25(1): 139–146 (in Chinese with English abstract).

Tan Fuwen, Zhang Runhe, Wang Jian, Si Chunsong and Ma Liqiao, 2016. Discussion on basement structures of the late Triassic-early Cretaceous Qiangtang rift basin in Tibet, China. *Journal of Chengdu University of Technology*, 43(5): 513–521 (in Chinese with English abstract).

Vervoort, J.D., and Blichert-Toft, J., 1999. Evolution of the depleted mantle: Hf isotope evidence from juvenile rocks through time. *Geochimica et Cosmochimica Acta*, 63(3–4): 533–556.

Wang Chenshan, Yi Haisheng, Li Yong, Deng Bin, Liu Dengzhong, Wang Guozhi, Shi He, Li Youguo, Ma Runze, and Lin Jinhui, 2001. *The Geological Evolution and Prospective Oil and Gas Assessment of the Qiangtang Basin in Northern Tibetan Plateau*. Beijing: Geological Publishing House, 1–249 (in Chinese).

Wang Jian, Tan Fuwen, Li Yalin, Li Yongtie, Chen Ming, Wang Chengshan, Guo Zujun, Wang Xiaolong, Du Bowei and Zhu Zhongfa, 2004. *The Potential of the Oil and Gas Resources inMajor Sedimentary Basins on the Qinghai-Xizang Plateau*. Beijing: Geological Publishing House, 34–88 (in Chinese).

Wang Jian, Fu Xiugen, Chen Wenxi and Wang Zhengjiang, 2007a. The Late Triassic paleo-weathering crust in the Qiangtang basin, northern Tibet: geology, geochemistry and significance. *Acta Sedimentologica Sinica*, 25(4): 487–494 (in Chinese with English abstract).

Wang Jian, Wang Zhengjiang, Chen Wenxi, Fu Xiugen and Chen Ming, 2007b. New evidences for the age assignment of the Nadi Kangri Formation in the North Qiangtang basin, nor thern Tibet, China. *Geological Bulletin of China*, 26(4): 404–409 (in Chinese with English abstract).

Wang, J., Fu, X.G., Chen, W.X., Wang, Z.J., Tan, F.W., Chen, M., and Zhuo, J.W., 2008. Chronology and geochemistry of the volcanic rocks in Woruo mountain region, northern Qiangtang depression: implications to the Late Triassic volcanic-sedimentary events. *Science in China series: Earth Science*, 51(2): 194–205.

Wang Jian, Ding Jun, Wang Chenshan, Tan Fuwen, Chen Ming, Hu Ping and Li Yain, 2009. *Investigation and evaluation of the Qinghai-Tibet Plateau oil and gas resources strategy constituency*. Beijing: Geological Publishing House, 19–200 (in Chinese).

Wang Jian, Fu Xiugen, Tan Fuwen, He Jianglin and Chen Ming, 2010. A New Sedimentary Model for the Qiangtang Basin. *Acta Sedimentologica Sinica*, 28(5): 884–893.

Wang Jian and Fu Xiugen, 2018. Discussion on the sedimentary evolution of the Qiangtang Basin. *Chinageology*, 45(2): 237–259 (in Chinese with English abstract).

Wu, F.Y., Yang, Y.H., Xie, L.W., Yang, J.H., and Xu, P., 2006. Hf isotopic compositions of the standard zircons and baddeleyites used in U-Pb geochronology. *Chemical Geology*, 234: 105–126.

Wu, H., Li, C., Chen, J.W., and Xie, C.M., 2015. Late Triassic tectonic framework and evolution of Central Qiangtang, Tibet, SW China. *Lithosphere*, 8(2): 141–149.

Yin, A., and Harrison, T.M., 2000. Geologic evolution of the

Himalayan-Tibetan orogeny. *Annual Review of Earth and Planetary Sciences*, 28(28): 211–280.

Zhai Qingguo and Li Cai, 2007. Zircon SHRIMP dating of volcanic rock from the Nadigangri Formation in Juhuashan, Qiangtang, northern Tibet and its geological significance. *Acta Geologica Sinica*, 81(6): 795–800 (in Chinese with English abstract).

Zhai, Q.G., Jahn, B.M., Su, L., Wang, J., Mo, X.X., Lee, H.Y., Wang, K.L., and Tang, S.H., 2013. Triassic arc magmatism in the Qiangtang area, northern Tibet: zircon U-Pb ages, geochemical and Sr-Nd-Hf isotopic characteristics, and tectonic implications. *Journal of Asian Earth Sciences*, 63: 162–178.

Zhao, Z.Z., and Li, Y.T., 2000. Conditions of petroleum geology of the Qiangtang Basin of the Qinghai-Tibet plateau. *Acta Geologica Sinica (English Edition)*, 74(3): 661–665.

Zhao Zhengzhang, Li Yongtie, Ye Hefei and Zhang Yuwen, 2000. *Oil and Gas Generation of Mesozoic Marine Source Rock in the Qinghai-xizang Plateau, China*. Beijing: Science Press, 1–214 (in Chinese).

Zhu Tongxing, Feng Xintao and Liu Shiliang, 2012a. *Regional Geological Report of Heihuling Sheet (1:250000)*. Wuhan: China University of Geosciences Press, 1–223 (in Chinese).

Zhu Tongxing, Li Zongliang and Zhang Huihua, 2012b. *Regional Geological Report of Jiangaidarina Sheet (1:250000)*. Wuhan: China University of Geosciences Press, 1 –332 (in Chinese).

Zhu Tongxing, Pan Zhongxi, Zhuang Zhonghai, Qin Jianhua, Dong Wentong, Wang Xiaolong, Huang Zhiying and Feng Xintao, 2002. Magnetostratigraphic Study of the Marine Jurassic in the Shuanghu Area, Northern Tibet. *Acta Geologica Sinica*, 76(3): 308–316 (in Chinese with English abstract).

About the first author

LI Xueren Male; born in 1986; A PhD candidate from the Chinese Academy of Geological Sciences and the China University of Geosciences (Beijing); He is currently interested in the study of sedimentology and petroleum geology. Email: xueren.li@foxmail.com; phone: 18200122505.